

# A 1-hole Cu<sub>4</sub>S cluster with N<sub>2</sub>O reductase activity: a structural and functional model for Cu<sub>Z</sub>\*

Brittany J. Johnson, William E. Antholine, Sergey V. Lindeman, Michael J. Graham,  
Neal P. Mankad\*

\* npm@uic.edu

## Supporting Information

### Contents:

Experimental and preparation of compounds	S3
Reaction between <b>2</b> and N <sub>2</sub> O	S7
Oxygen trapping experiments from reaction between <b>2</b> and N <sub>2</sub> O	S8
Headspace Analysis by GC-MS of <sup>15</sup> N <sub>2</sub> O and <b>2</b>	S9
Computational methods	S10
Figure S1. $\chi T$ vs. temperature plots of <b>1</b> <sup>4</sup>	S12
Figure S2. X-ray crystal structure of Cu(II)S <sub>2</sub> NCN <sub>2</sub> paramagnetic impurity	S13
Figure S3. X-band EPR spectrum of Cu(II)S <sub>2</sub> NCN <sub>2</sub> impurity	S14
Figure S4. Q-band EPR spectrum of <b>2</b>	S15
Figure S5. X-band EPR spectrum of <b>2</b>	S16
Figure S6. <sup>1</sup> H NMR of <b>2</b>	S16
Figure S7. Absorption spectra for 0.082 mM <b>2</b> and 0.085 mM <b>1</b> <sup>4</sup> in THF	S17
Figure S8. Infrared spectrum of <b>2</b>	S18
Figure S9. <sup>1</sup> H NMR of <b>1</b> formed after exposure of N <sub>2</sub> O to <b>2</b>	S19
Figure S10. <sup>1</sup> H NMR of control experiment between N <sub>2</sub> and <b>2</b>	S20
Figure S11. <sup>1</sup> H NMR of recovered <b>1</b> after reaction with N <sub>2</sub> O and <b>2</b>	S21
Figure S12. <sup>1</sup> H NMR of recovered <b>1</b> after control between N <sub>2</sub> and <b>2</b>	S22
Figure S13. <sup>1</sup> H NMR of oxygen trapping using Me <sub>3</sub> SiCl after N <sub>2</sub> O and <b>2</b>	S23
Figure S14. <sup>1</sup> H NMR of oxygen trapping using Me <sub>3</sub> SiCl after N <sub>2</sub> and <b>2</b>	S24

Figure S15. $^1\text{H}$ NMR of oxygen trapping using benzoyl chloride after $\text{N}_2\text{O}$ and <b>2</b>	S25
Figure S16. Comparison of $^1\text{H}$ NMR of oxygen trapping using benzoyl chloride to confirm formation of benzoic anhydride	S26
Figure S17. Reaction headspace chromatogram from $^{15}\text{N}_2\text{O}$ and <b>2</b>	S27
Figure S18. $^{15}\text{N}_2\text{O}$ blank flask chromatogram	S28
Figure S19. Mass spectrum of $^{15}\text{N}_2\text{O}$ and <b>2</b> after 48 hours	S29
Table S1. Percent composition of species in Figure S19	S29
Figure S20. Mass spectrum of $^{15}\text{N}_2\text{O}$ blank after 48 hours	S30
Table S2. Percent composition of species in Figure S20	S30
Figure 21. Mass spectrum of $^{15}\text{N}_2\text{O}$ and <b>2</b> after 6 hours	S31
Table S3. Percent composition of species in Figure S21	S31
Figure S22. Mass spectrum of $^{15}\text{N}_2\text{O}$ blank	S32
Table S4. Percent composition of species in Figure S22	S32
Figure S23. Mass spectrum of elude at 5.48 minutes in Figure S17	S33
Table S5. Integration values of $^{15}\text{N}_2$ from reaction vs. blank headspace	S33
Table S6: Comparison of calculated and experimental bond distances	S34
Figure S24. Optimized structure of <b>2'</b>	S35
Figure S25. Calculated UV-Vis spectrum of <b>2'</b>	S35
Figure S26. Optimized structure of <b>1'</b>	S36
Figure S27. Calculated UV-Vis spectrum of <b>1'</b>	S36
Table S7. Optimized coordinates of <b>2'</b>	S37
Table S8. Optimized coordinates of <b>1'</b>	S39
Table S9. Excitation energies and oscillator strengths of <b>2'</b>	S41
Table S10. Excitation energies and oscillator strengths of <b>1'</b>	S45
Figures S28-29. Selected MO surfaces for <b>1'</b>	S52
Figures S30-31. Selected MO surfaces for <b>2'</b>	S53
References cited	S54

## EXPERIMENTAL

**General Considerations.** Unless otherwise specified, all reactions and manipulations were performed under purified N<sub>2</sub> in a glovebox or using standard Schlenk line techniques. Glassware was oven-dried prior to use. Reaction solvents (diethyl ether, toluene, tetrahydrofuran, dichloromethane, acetonitrile, pentane) were sparged with argon and dried using a Glass Contour Solvent System built by Pure Process Technology, LLC. Deuterated solvents were degassed by repeated freeze-pump-thaw cycles and then stored over 3-Å molecular sieves. Unless otherwise specified, all other chemicals were purchased from commercial sources and used without further purification. 1 L of Nitrous Oxide (<sup>15</sup>N<sub>2</sub>, 98%+) was purchased from Cambridge Isotope Laboratories, Inc. A 460 mL Stainless Steel 1/4" NPT Stainless Steel Whitey Straight/Male adaptor was also purchased and assembled from Cambridge Isotope Laboratories packaging prior to shipment.

**Spectroscopic Measurements.** NMR spectra for compound characterization were recorded at ambient temperature using Bruker Avance DPX-400 or Bruker Avance DRX-500 MHz spectrometers. <sup>1</sup>H NMR chemical shifts were referenced to residual solvent peaks. FT-IR spectra were recorded on solid samples in a glovebox using a Bruker ALPHA spectrometer fitted with a diamond-ATR detection unit. Elemental analyses were performed by the Midwest Microlab, LLC in Indianapolis, IN. UV-Vis absorbance spectra were taken at room temperature using a JASCO V-660 Spectrophotometer. Absorbance was measured at 0.5 nm intervals and with a continuous scan speed of 1000 nm/min. X-band spectra were obtained at 10 K with an Elexsys E500 spectrometer, Bruker, Billerica, MA located at the National Biomedical EPR Center at the Medical College of Wisconsin. Q-band spectra were obtained on a Varian E109 spectrometer at -150°C located at the National Biomedical EPR Center at the Medical College of Wisconsin. Spectra were

simulated with EasySpin.<sup>1</sup> The 1st harmonic spectra were obtained using SumSpec (a program available from the National Biomedical EPR Center) using pseudomodulation with a 1% or 3% Bessel function. Samples of 5 mM **1**<sup>4</sup> (not shown), **2** and Cu(II)S<sub>2</sub>NCN<sub>2</sub>-containing impurity were glassed in 2-methyltetrahydrofuran.

**Magnetic Measurements.** Magnetic measurements were performed on polycrystalline samples in a sealed polyethylene bag or in a sealed quartz tube restrained with eicosane. All data were collected using a Quantum Design MPMS-XL SQUID magnetometer in a temperature range of 1.8 to 400 K at applied dc fields of 0.1 T and 7 T. A quartz tube was employed for high temperature measurements to avoid melting the polyethylene bag, and a high-field was employed with the quartz-tube sample to ensure sufficient signal-to-noise at high temperatures.

**X-ray crystallography.** X-ray crystallography data on dark violet tablets of **2** was collected at the X-ray Structural Laboratory at Marquette University (Milwaukee, WI). The X-ray single-crystal diffraction data were collected with an Oxford Diffraction SuperNova diffractometer equipped with dual microfocus Cu/Mo X-ray sources, X-ray mirror optics, Atlas CCD detector and low-temperature Cryojet device. Data was collected using Cu(K $\alpha$ ) radiation at 100 K. The data was processed with CrysAlisPro program package (Oxford Diffraction Ltd., 2010) typically using a numerical Gaussian absorption correction (based on the real shape of the crystal) followed by an empirical multi-scan correction using SCALE3 ABSPACK routine. The structures were solved using SHELXS program and refined with SHELXL program<sup>2</sup> within Olex2 crystallographic package.<sup>3</sup> All computations were performed on an Intel PC computer under Windows 7 OS. Hydrogen atoms were localized in difference syntheses of electron density but were refined using appropriate geometric restrictions on the corresponding bond lengths and bond angles within a riding/rotating model (torsion angles of Me hydrogens were optimized to better fit

the residual electron density). The crystal was twinned: regular twins with  $180^\circ$  rotation around direct  $-101$  vector. Because of quasi-rational cell dimensions, all reflections with  $h+l=2n$  overlap exactly (but not with identical indexes - HKL transformation matrix  $\begin{pmatrix} -.5 & 0 & -.5 & 0 & -1 & 0 & -1.5 & 0 & .5 \end{pmatrix}$ ). Reflections with  $h+l=2n+1$  are separate. The structure contains two symmetrically independent tetranuclear units having a similar geometry. Two  $K^+$ /18-crown-6 counter ions are disordered to a different degree. The disorder affects as the position of K atom (swinging alternatively in axial direction to make  $K^+ \dots Ar$  contacts with neighboring anions) as well as the crown-ether itself. The structure contains well-ordered 1 eq of solvate DCM solvent. It also contains large areas of highly-disordered solvent only partially localized/identified as diethyl ether. Because of the twinning, an application of a solvent mask procedure was prohibited.

**Headspace Analysis by GC-MS.** Headspace gas was analyzed by a JEOL GCMate II (JEOL USA, Peabody MA) gas chromatograph/mass spectrometer, the gas chromatograph was an Agilent 6890Plus (Wilmington DE) equipped with a G1513A autoinjector with 100 vial sample tray connected to a G1512A controller. The gas chromatography column was a J&W GS-CarbonPLOT (Agilent Tech), 60 m long, 0.320 mm diameter, 1.50  $\mu\text{m}$  film thickness. The carrier gas was helium (99.999% Ultra High Purity) run through a STG triple filter (Restek Corp.) at a constant flow rate of 2.5 mL/min. The inlet temperature was  $250^\circ\text{C}$  and was fitted with an Agilent 4 mm ID single taper split liner containing deactivated glass wool. The static headspace analysis was performed using 5  $\mu\text{L}$  of the experimental gas mixture manually injected via syringe. The GC inlet split ratio was 20:1. The GC oven was run in isothermal mode at a temperature of  $30^\circ\text{C}$  for 5 minutes then ramped  $10^\circ\text{C}/\text{min}$  to  $80^\circ\text{C}$ . Total run time was approximately 10 min. The mass spectrometer was a benchtop magnetic sector operating at a nominal resolving power of 500 using an accelerating voltage of 2500 V. The spectrometer was operated in full scan EI mode (+Ve) with

the filament operating at 70 eV scanning from  $m/z$  10 to  $m/z$  850 using a linear magnet scan. The scan speed was 0.2 s/scan. Data analysis was performed using the TSSPro software (Shrader Analytical & Consulting Laboratories, Inc., Detroit MI) provided with the spectrometer. Mass calibration was performed using perfluorokerosene (PFK).

**Preparation of  $[\text{Cu}_4(\mu_4\text{-S})(\mu_2\text{-NCN})_4][\text{K}(18\text{-crown-6})]$  (**2**).** **1**<sup>4</sup> (0.10 g, 0.079 mmol) was dissolved in approximately 60 mL of toluene using a magnetic stir bar. Solid  $[\text{K}(18\text{-crown-6})_2][\text{Fp}]^5$  (0.057 g, 0.076 mmol) was added slowly to stirring solution at room temperature. The solution was stirred vigorously overnight. The next day the solution was filtered. The collected dark solid was washed with pentane to remove any  $\text{Fp}_2$  (cyclopentadienyliron dicarbonyl dimer) until filtrate was clear, and then washed with toluene to remove any unreacted **1** until filtrate was clear. The solid was collected and dried under vacuum. Yield of **2**: 0.091 g, 75%. Compound **2** was stored in a freezer ( $-36^\circ\text{C}$ ) and is not stable in solution at room temperature for more than an hour. Note: Trace amounts (2-5%) of  $\text{Cu}_2[(2,4,6\text{-Me}_3\text{C}_6\text{H}_2\text{N})_2\text{C}(\text{H})_2]^4$  were often detected by <sup>1</sup>H NMR regardless of multiple purification attempts. The best method for removing  $\text{Cu}_2[(2,4,6\text{-Me}_3\text{C}_6\text{H}_2\text{N})_2\text{C}(\text{H})_2]$  is by adding a small amount of tetrahydrofuran (2 mL) to solid **2** (0.091 g) so that  $\text{Cu}_2[(2,4,6\text{-Me}_3\text{C}_6\text{H}_2\text{N})_2\text{C}(\text{H})_2]$  dissolves but **2** is super-saturated and doesn't dissolve entirely. This solution is filtered, and the resulting purple solid is washed with a small amount of tetrahydrofuran (2 mL) and then pentane (2 mL) to remove any remaining tetrahydrofuran solvent. The purple solid can then be collected and dried under vacuum. Usually this purification method is done once to achieve experimental purity. Dark black crystals may be obtained by dissolving **2** in a minimum amount of dimethoxyethane, pipette-filtering through Celite, and leaving solution at  $-36^\circ\text{C}$  for four days. NMR samples were dissolved in acetone-*d*<sub>6</sub> and pipette-filtered through Celite into NMR tube. <sup>1</sup>H NMR (500 MHz, acetone-*d*<sub>6</sub>):  $\delta$  3.66 (s, 24 H, 18-crown-6). FT-IR (cm<sup>-1</sup>

<sup>1</sup>): 2992, 2903, 2854, 2724, 1717, 1652, 1609, 1556, 1538, 1469, 1330, 1209, 1104, 959, 847, 738, 586, 504, 422. Anal. calcd. for C<sub>88</sub>H<sub>116</sub>Cu<sub>4</sub>N<sub>8</sub>O<sub>6</sub>SK: C, 61.90; H, 6.85; N, 6.56. Found: C, 60.37; H, 6.50; N, 6.57. Repeated attempts at obtaining satisfactory combustion analysis results (with %C within ±0.4% of the calculated value) gave results with a large degree of variance, indicating either that the spectroscopically pure samples were compromised during shipping/handling or that the compound does not combust cleanly.

**Detection of 1 after reaction between N<sub>2</sub>O and 2.** Inside a N<sub>2</sub> filled glovebox, to a Schlenk tube equipped with a Teflon screw cap and magnetic stir bar, **2** (0.006 g, 0.0035 mmol) was added and dissolved in approximately 2.5 mL dichloromethane. The tube was sealed with the Teflon screw cap and taken out of the glovebox and connected to a Schlenk line streaming N<sub>2</sub>O. The solution was cooled to -78° C (dry ice and acetone bath) with stirring. The solution was then exposed to N<sub>2</sub>O for 6.5 hours while maintaining the cooling bath at -78° C. Once cooling bath was removed, solvent was removed by vacuum evaporation and Schlenk tube was closed and pumped back into the glovebox. Evaporated residue was dissolved in CD<sub>2</sub>Cl<sub>2</sub> and pipette-filtered through Celite into an NMR tube for analysis. A control experiment was conducted by same procedure using 0.005 g (0.0029 mmol) of **2** in approximately 2 mL of dichloromethane while under N<sub>2</sub>. Using integration of 18-crown-6 as an internal standard (24 H) in <sup>1</sup>H NMR reveals 45% NMR yield of **1**<sup>4</sup> in the reaction with N<sub>2</sub>O (Figure S9) with respect to any Ar-CH<sub>3</sub> peak of **1** (12 H) and 0% yield in N<sub>2</sub> control experiment (Figure S10).

**Recovery of 1 after reaction between N<sub>2</sub>O and 2.** Inside a N<sub>2</sub> filled glovebox, to a Schlenk tube equipped with a Teflon screw cap and magnet stir bar, **2** (0.021 g, 0.012 mmol) was added and dissolved in dichloromethane (10 mL). The tube was sealed with the Teflon cap and taken out of the glovebox and connected to Schlenk line streaming with N<sub>2</sub>O. The solution in the

flask was cooled to  $-78^{\circ}\text{C}$  (dry ice and acetone bath) with stirring, and then opened to  $\text{N}_2\text{O}$  for 6 hours while maintaining the cooling bath at  $-78^{\circ}\text{C}$ . Solvent was removed by vacuum evaporation and Schlenk tube was closed and pumped back into the glovebox. Purple evaporated residue inside Schlenk tube was washed with acetonitrile (approximately 20 mL), in which **1** is insoluble, and then pipette-filtering through Celite until filtrate became clear. Dark purple solid remaining was collected using dichloromethane and the solution was completely evaporated by vacuum. The same procedure was followed in a control experiment using 0.021 g (0.012 mmol) of **2** in 10 mL of dichloromethane under  $\text{N}_2$ . Amount of **1** isolated from  $\text{N}_2\text{O}$  reaction residue: 0.015 g (0.010 mmol, 88% yield, Figure S11); amount of **1** isolated from  $\text{N}_2$  control reaction residue: 0.0052 g (0.0035 mmol, 30% decomposition, Figure S12).

**Oxygen Trapping Experiment with  $\text{Me}_3\text{SiCl}$ .** Inside a  $\text{N}_2$  filled glovebox, to a Schlenk tube equipped with a Teflon screw cap and magnet stir bar, **2** (0.003 g, 0.0017 mmol) was added and dissolved in dichloromethane (3 mL). The tube was sealed with the Teflon cap and taken out of the glovebox and connected to Schlenk line streaming with  $\text{N}_2\text{O}$ . The solution in the flask was cooled to  $-78^{\circ}\text{C}$  (dry ice and acetone bath) with stirring, and then opened to  $\text{N}_2\text{O}$  for 3.5 hours while maintaining the temperature at  $-78^{\circ}\text{C}$ . Solvent was removed by vacuum evaporation and Schlenk tube was closed and pumped back into the glovebox. Purple evaporated residue inside Schlenk tube was dissolved in approximately 1 mL of  $\text{CD}_2\text{Cl}_2$ , and 95  $\mu\text{L}$  of a 0.092 M solution of TMS-Cl (0.0087 mmol) in  $\text{CD}_2\text{Cl}_2$  was added. Contents were stirred for 1 hour at room temperature and were then pipette-filtered through Celite into an NMR tube for analysis (Figure S13). The same procedure was followed in a control experiment using 0.006 g (0.0035 mmol) of **2** in 3 mL of dichloromethane, under  $\text{N}_2$ , followed by addition of 190  $\mu\text{L}$  of 0.092 M TMS-Cl in  $\text{CD}_2\text{Cl}_2$  solution (0.017 mmol) in the same manner as described in the  $\text{N}_2\text{O}$  experiment (Figure

S14).  $^1\text{H}$  NMR (400 MHz,  $\text{CD}_2\text{Cl}_2$ ):  $\delta$  0.07 (s,  $(\text{Me}_3\text{Si})_2\text{O}$ ), 0.43 (s, unreacted TMS-Cl), 1.31 (s, **1** Ar- $\text{CH}_3$ ), 1.39 (s, **1** Ar- $\text{CH}_3$ ), 2.15 (s, **1** Ar- $\text{CH}_3$ ), 2.17 (s, **1** Ar- $\text{CH}_3$ ), 2.69 (s, **1** Ar- $\text{CH}_3$ ), 2.77 (s, **1** Ar- $\text{CH}_3$ ), 3.63 (s, 18-crown-6), 6.10 (s, **1** NC(H)N), 6.25 (s, **1** Ar-CH), 6.31 (s, **1** Ar-CH), 6.61 (s, **1** NC(H)N), 6.71 (s, **1** Ar-CH).

**Oxygen Trapping Experiment with Benzoyl Chloride.** Inside a  $\text{N}_2$  filled glovebox, to a Schlenk tube equipped with a Teflon screw cap and magnet stir bar, **2** (0.010 g, 0.0058 mmol) was added and dissolved in dichloromethane (5 mL). The tube was sealed with the Teflon cap and taken out of the glovebox and connected to Schlenk line streaming with  $\text{N}_2\text{O}$ . The solution in the flask was cooled to  $-78^\circ\text{C}$  (dry ice and acetone bath) with stirring, and then opened to  $\text{N}_2\text{O}$  for 3 hours while maintaining the temperature at  $-78^\circ\text{C}$ . Solvent was removed by vacuum evaporation and Schlenk tube was closed and pumped back into the glovebox. Purple evaporated residue inside Schlenk tube was mixed with approximately 8 mL of diethyl ether and 20  $\mu\text{L}$  of a 0.287 M solution of cold ( $-32^\circ\text{C}$ ) benzoyl chloride (0.0057 mmol) in diethyl ether was added. Contents stirred for 1 hour at room temperature, pipette-filtered through Celite and solvent was removed by vacuum evaporation. Resulting residue was dissolved in  $\text{C}_6\text{D}_6$  and pipette-filtered through Celite into an NMR tube for analysis (Figure S15-S16).  $^1\text{H}$  NMR (400 MHz,  $\text{C}_6\text{D}_6$ ):  $\delta$  1.46 (s, **1** Ar- $\text{CH}_3$ ), 1.57 (s, **1** Ar- $\text{CH}_3$ ), 2.18 (s, **1** Ar- $\text{CH}_3$ ), 2.20 (s, **1** Ar- $\text{CH}_3$ ), 2.83 (s, **1** Ar- $\text{CH}_3$ ), 2.97 (s, **1** Ar- $\text{CH}_3$ ), 3.52 (s, 18-crown-6), 6.37 (s, **1** Ar-CH), 6.44 (s, **1** Ar-CH), 6.94 (m, benzoic anhydride Ar-CH), 7.07 (m, benzoic anhydride Ar-CH), 7.96 (m, benzoic anhydride Ar-CH).

**Reaction Headspace Analysis of  $^{15}\text{N}_2$  Produced from the Reaction between  $^{15}\text{N}_2\text{O}$  and **2**.** Inside a  $\text{N}_2$  filled glovebox, to a 100 mL round bottom Schlenk flask with a magnetic stir bar, **2** (0.125 g, 0.0732 mmol) was added and dissolved in THF (60 mL). The flask was sealed with a fresh septum secured with copper wire and a Keck clip. The flask was taken out of the glovebox

and connected to a T-shaped stopcock connected to a Schlenk line streaming both N<sub>2</sub> and <sup>15</sup>N<sub>2</sub>O gases. After five freeze-pump-thaw cycles, the flask was cooled to - 78° C (dry ice and acetone bath) and headspace was backfilled quickly with <sup>15</sup>N<sub>2</sub>O (~3 seconds) and then the flask was closed. The reaction was stirred at - 78° C for three hours, and then the cooling bath was removed. The reaction was then stirred for 3 hours at room temperature to equilibrate the gases in the reaction headspace and dissolved in the solution. The gases in the reaction headspace were then analyzed by 5 μL injections into GC-MS (Figure S21). After the 6 hour GC-MS headspace measurement, the reaction flask sat for 48 hours at room temperature, without stirring to prevent high pressure build-up within the flask. After 48 hours, the gases in the headspace were again analyzed by 5 μL injections into the GC-MS (Figures S17 and S19). To serve as a blank, a 50 mL round bottom Schlenk flask was sealed using a fresh septum secured with copper wire and a Keck clip. The blank flask was evacuated by vacuum and refilled with <sup>15</sup>N<sub>2</sub>O and then closed. Gases in blank flask were analyzed by a 5 μL injection (Figure S22). Blank flask then sat alongside the reaction flask for 48 hours at room temperature and was re-analyzed by GC-MS (Figure S18 and S20).

**Computational Methods.** All calculations were performed using Gaussian09, Revision B.01.<sup>6</sup> Density functional theory (DFT) calculations were carried out using the B3LYP functional.<sup>7</sup> Mixed basis sets were employed: the LANL2TZ(f) triple- $\zeta$  basis set<sup>8</sup> with effective core potential<sup>9</sup> was used for Cu, the Gaussian09 internal 6-311+G(d) basis set was used for S, and the Gaussian09 internal 6-31+G(d) basis set was used for C, H, and N. All calculations included a polarizable continuum model for dichloromethane solvation.<sup>10</sup> The optimized coordinates for model **1'** (where the mesityl groups of **1** were replaced with methyls) at a slightly different level of theory were reported previously<sup>4</sup> and were used as the starting point for obtaining optimized coordinates for neutral **1'** and anion **2'** (where the mesityl groups of **2** were replaced with methyls). Optimized

coordinates for both structures are enclosed below (Tables S2 and S3), along with comparisons of **1'** and **2'** to the experimental structures of **1** and **2** (Table S1). These optimized coordinates were used for single-point TD-DFT calculations (35 states for **1'**, 25 states for **2'**) at the same level of theory (see Figures S18-19). Lists of these transitions are included as Tables S4 and S5 below. Natural transition orbital analysis<sup>11</sup> was used to examine the nature of the dominant transition (State 9, 578 nm, 6000 M<sup>-1</sup>cm<sup>-1</sup>) in the predicted electronic spectrum of **2'**. The broken-symmetry S=0 and S=1 states of **1'** were found to be higher energy than the closed-shell S=0 state presented here, although all three states were within  $\pm 2$  kcal/mol of each other, indicating that high-level calculations are in order to accurately model **1**. Orbital surfaces and Mulliken spin density were plotted using Gaussview 4.1<sup>12</sup> and are presented with isovalues indicated in figure captions.

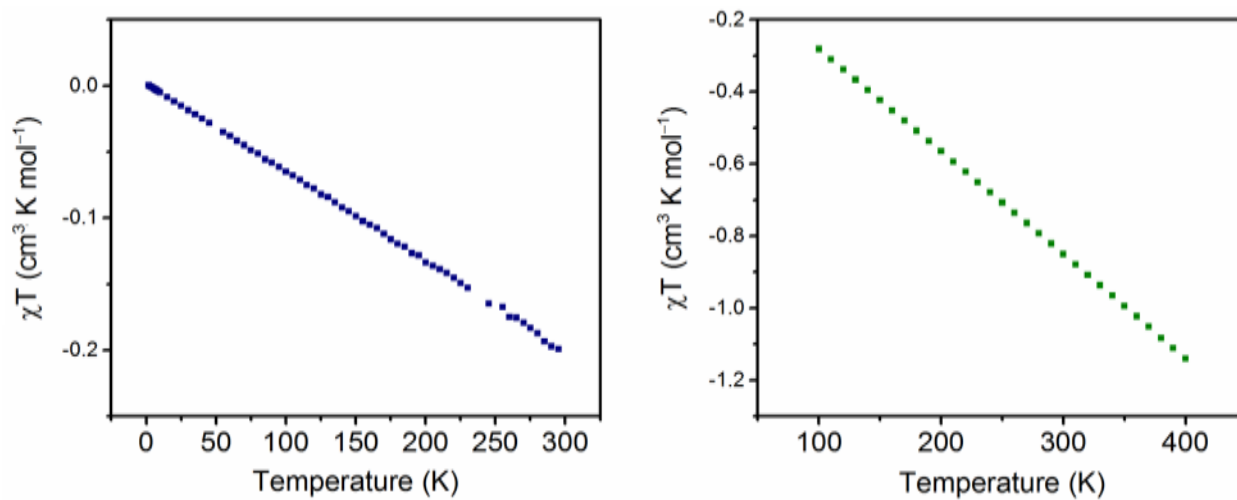


**Figure S1.**  $\chi T$  vs. temperature plots of **1**<sup>4</sup> in a polyethylene bag at a field of 0.1 T (left) and a separate sample of **1** in a sealed quartz tube at a field of 7 T (right). Both depict a downward-sloping, linear curve, indicative of a diamagnetic sample. The significantly larger diamagnetic moment exhibited by the quartz-tube sample (right) is attributable to the additional mass of the quartz and eicosane.

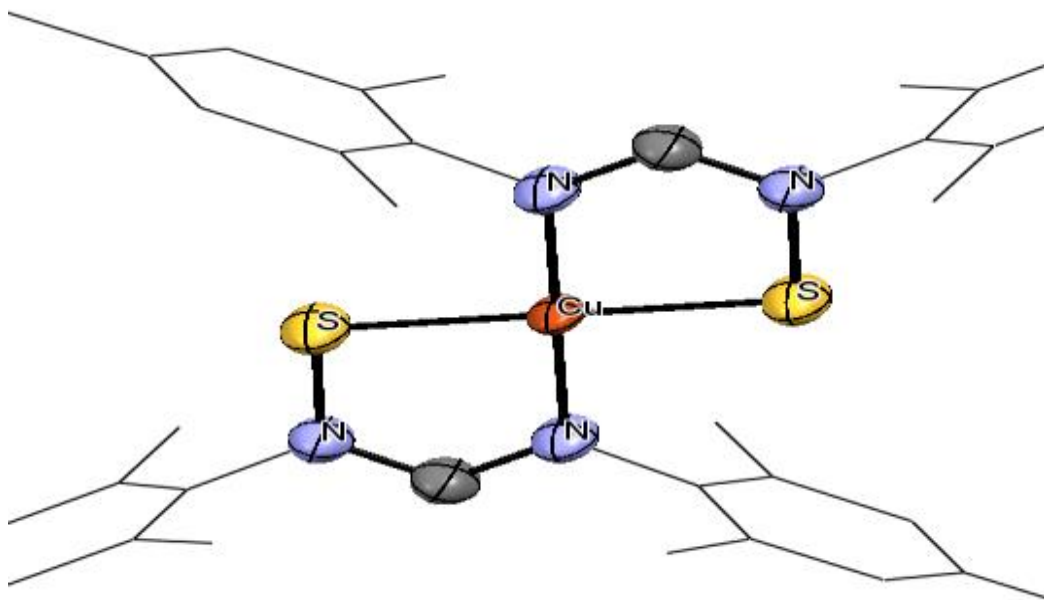


**Figure S2.** Solid state structure of Cu(II)S<sub>2</sub>NCN<sub>2</sub> paramagnetic impurity determined by single-crystal X-ray diffraction. Mesityl groups are shown as wireframes and other atoms are displayed as 50% probability thermal ellipsoids. Hydrogen atoms have been omitted. Cu(II)S<sub>2</sub>NCN<sub>2</sub> was isolated following the procedure published for **1**<sup>4</sup> by S<sub>8</sub> with the following modifications: the reaction mixture was stirred for two days at r.t. The crude reaction solution was filtered through Celite and the filtrate was completely evaporated by vacuum. Recrystallization by vapor diffusion of the filtrate residue in CHCl<sub>3</sub> and pentane vapors leads to formation of maroon crystals.

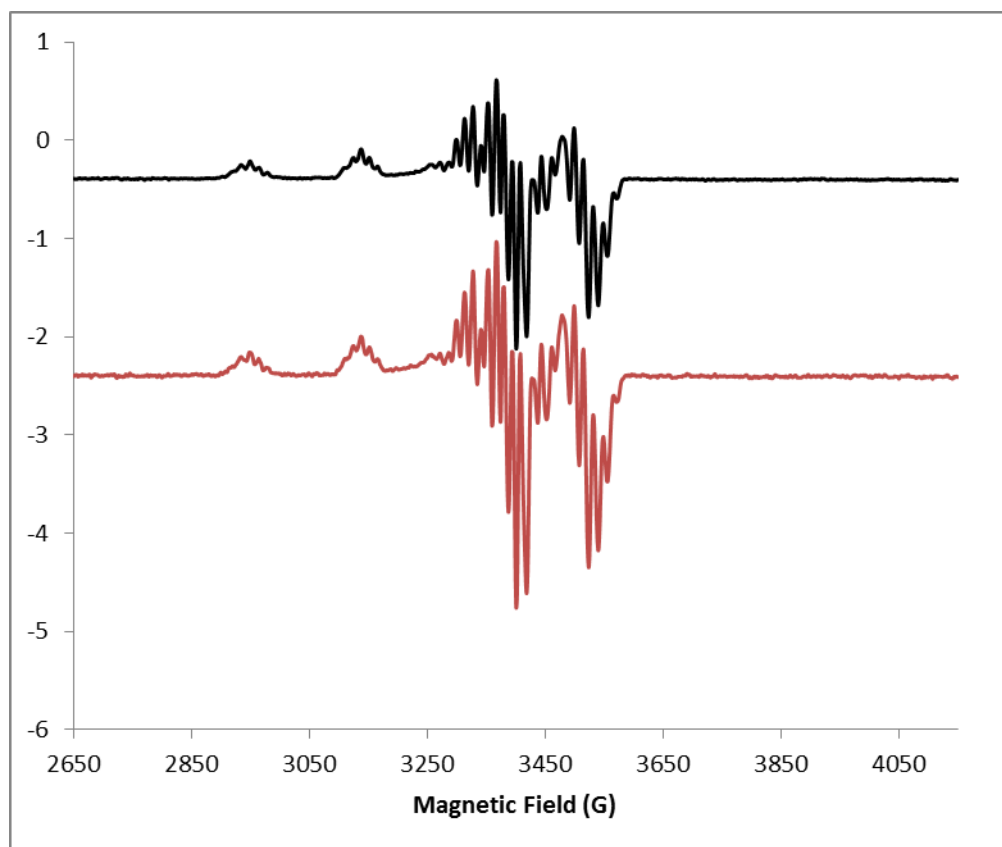


**Figure S3.** X-band EPR spectrum of the  $\text{Cu(II)S}_2\text{NCN}_2$  species from Figure S2 at 34 K (black trace) and 24 K (red trace), power 46 dB.

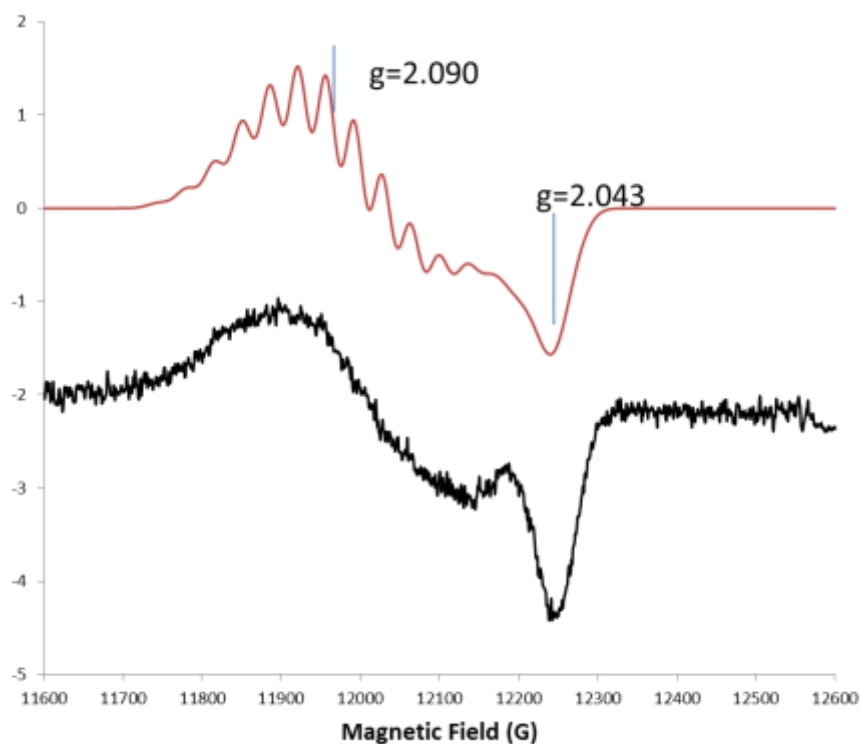


**Figure S4.** Q-band EPR spectrum for **2** (black scan): 34.99 GHz, -150 °C, 9 scans, power 22 dB, 10 G, mod.; time constant 0.1 sec; 2 min scans; Simulation (EasySpin, red scan):  $g=2.09$ , 2.043; four Cu's (both isotopes),  $A=100$ , 15 MHz;  $lwpp=0.5$ ;  $HStrain=100$  90.  $P_{1/2}$ , the power for which the X-band EPR signal is one-half of the expected signal if unsaturated, is 22.5 dB at 10 K and 26.5 dB at 5 K. The spin-lattice relaxation time is faster for mixed valence complexes in both **2** and  $Cu_Z$  than for monomeric cupric complexes. The difference in the EPR spectra between **2** and  $Cu_Z$  is most easily seen in the Q-band spectrum, where  $g \gt g_{ll}$  for **2**, but  $g \lt g_{ll}$  for  $Cu_Z$  (P. Cheng...E.J. Solomon, J. Am. Chem. Soc., 124(5),744,2002) suggesting that the unpaired electron in **2** is not a pure  $dx^2-y^2$  orbital. The line width for  $g_{ll}$  in the Q-band spectrum and simulations are used to approximate  $A_{ll}$ .  $A_{ll}$  is obtained from resolved lines in the X-band spectrum and from simulations. Another difference between **2** and  $Cu_Z$  is that the spectra for **2** are simulated with four equivalent coppers and the spectra for  $Cu_Z$  are simulated with two sets of inequivalent coppers.

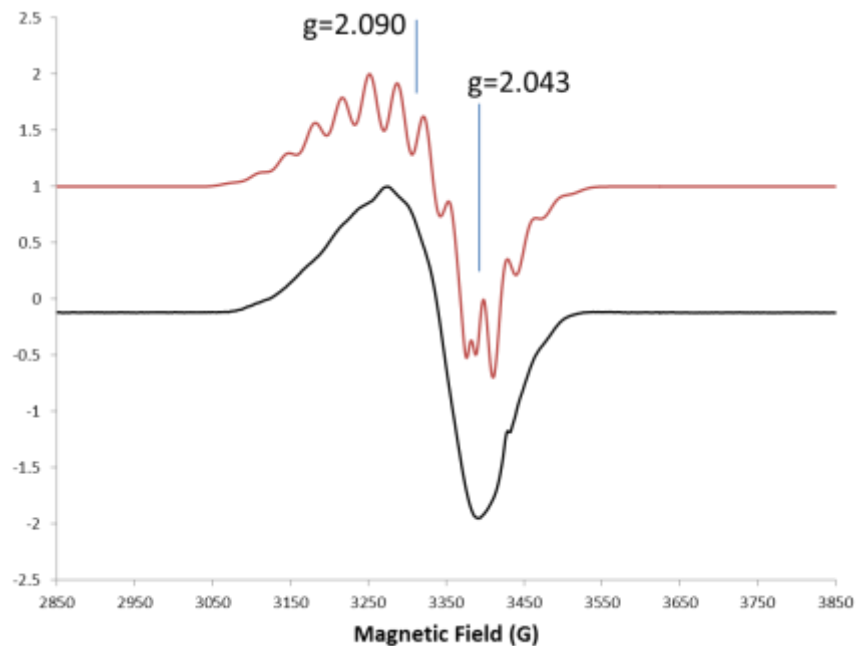


**Figure S5.** X-band EPR spectrum of **2** (black scan): 9.632 GHz, 9.9 K, 9 scans, power 46 dB; Simulation (red scan, EasySpin):  $g = 2.09, 2.043$ ; both 63 and 65 isotopes,  $A = 100, 15$  MHz,  $lwpp=0.5$ ;  $Hstrain:100\ 20$ .

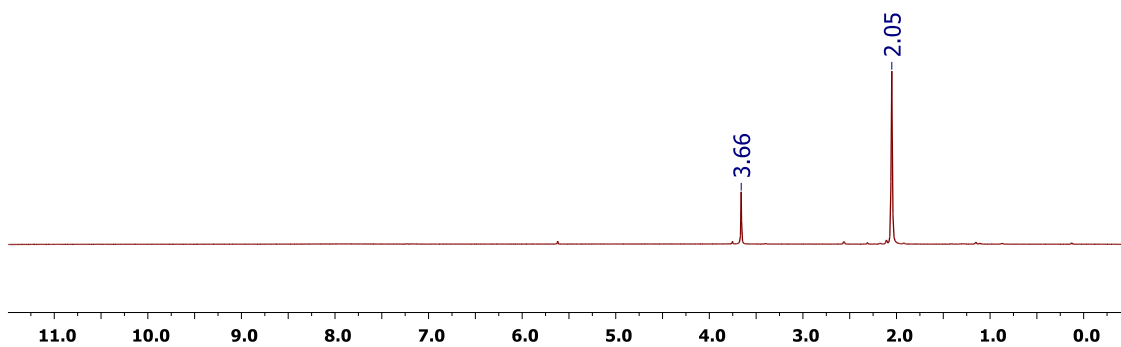


**Figure S6.**  $^1\text{H}$  NMR (500 MHz) of **2** in Acetone- $d_6$ .

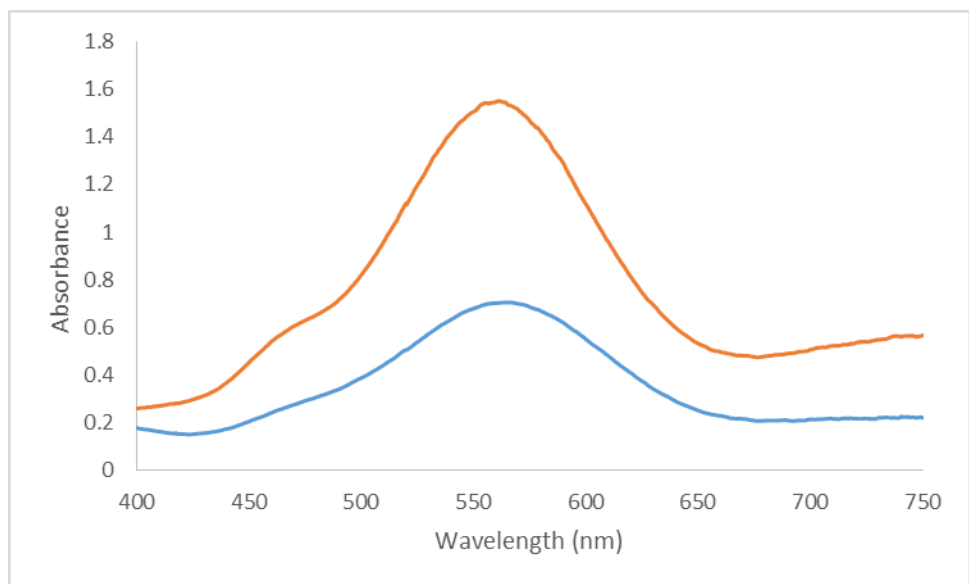


**Figure S7.** Absorption Spectra for 0.082 mM **2** (blue trace; absorption maxima at 565.5 nm;  $\epsilon = 8601 \text{ M}^{-1}\cdot\text{cm}^{-1}$ ) and 0.085 mM **14** (orange trace; absorption maxima at 561 nm;  $\epsilon = 18132 \text{ M}^{-1}\cdot\text{cm}^{-1}$ ) in THF at room temperature.

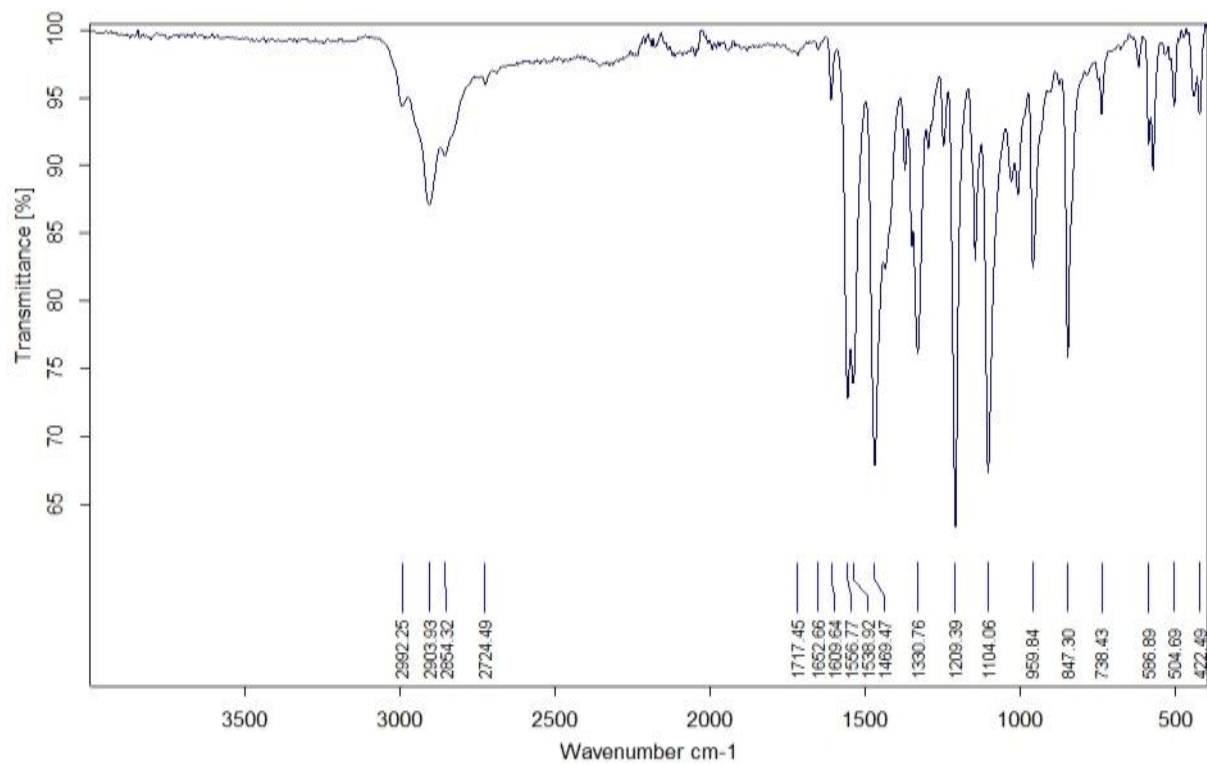


**Figure S8.** Infrared Spectrum of **2**.

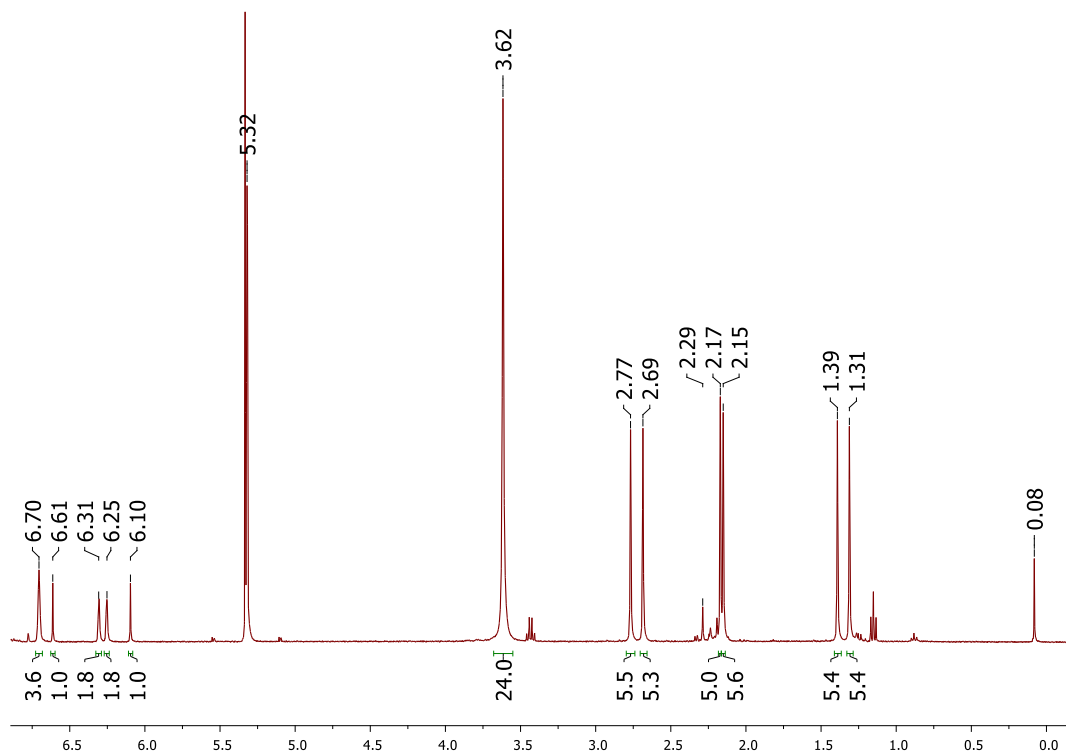


**Figure S9.**  $^1\text{H}$  NMR (400 MHz,  $\text{CD}_2\text{Cl}_2$ ) of reaction products from **2** +  $\text{N}_2\text{O}$  with appearance of **1** in 45% yield compared to integration of 18-crown-6 as the internal standard. Residual solvents in spectra are not peak picked. Peak appearing at 2.29 ppm is a decomposition product of **2**,  $\text{Cu}_2[(2,4,6\text{-Me}_3\text{C}_6\text{H}_2\text{N})_2\text{C}(\text{H})]_2^4$ .

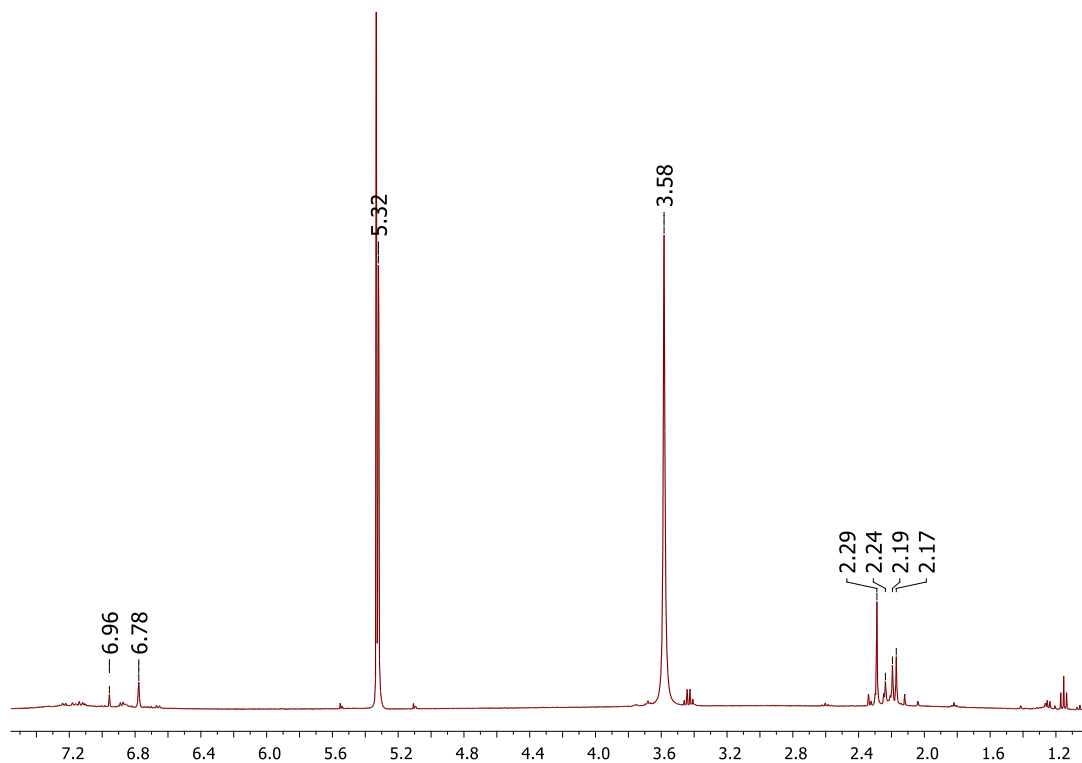


**Figure S10.** <sup>1</sup>H NMR (400 MHz, CD<sub>2</sub>Cl<sub>2</sub>) of control experiment between **2** and N<sub>2</sub>. Residual solvents in spectra are not peak picked. Peaks appearing at 2.17- 2.29 ppm and 6.78- 6.96 ppm are decomposition products of **2**; Cu<sub>2</sub>[(2,4,6-Me<sub>3</sub>C<sub>6</sub>H<sub>2</sub>N)<sub>2</sub>C(H)]<sub>2</sub><sup>4</sup> and free ligand (bis(2,4,6-trimethylphenyl)formamidine)<sup>4</sup>. No presence of **1** is evident.

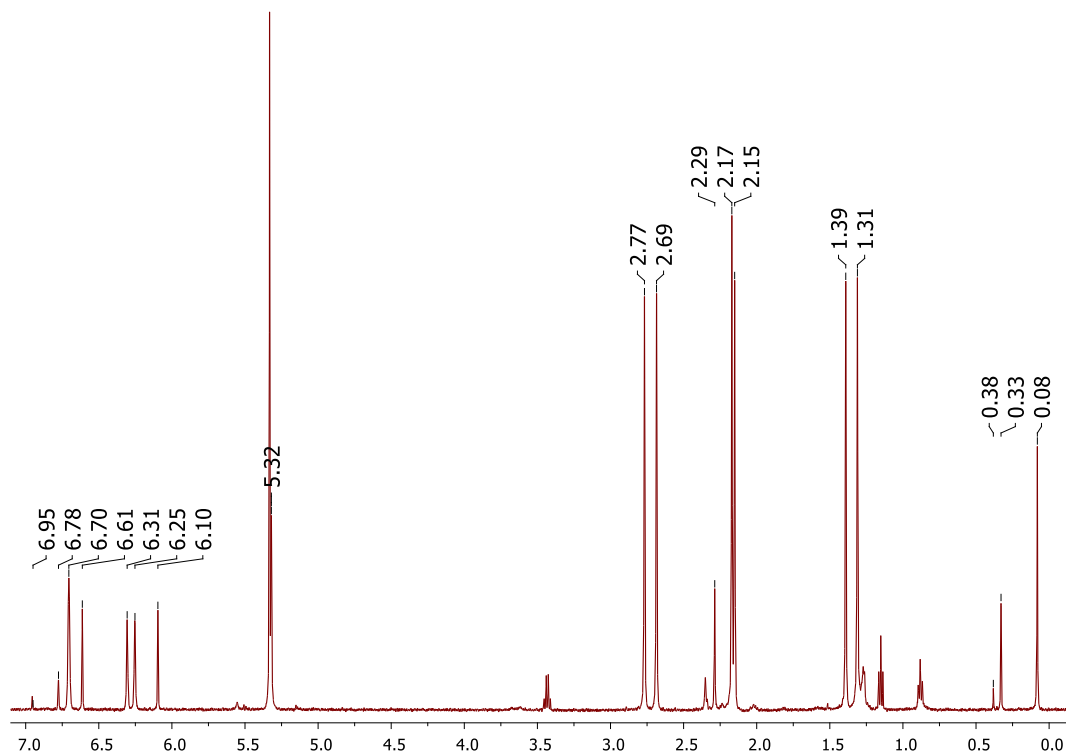


**Figure S11.**  $^1\text{H}$  NMR (500 MHz,  $\text{CD}_2\text{Cl}_2$ ) of **1** isolated after reaction between **2** and  $\text{N}_2\text{O}$  in  $\text{CD}_2\text{Cl}_2$  (88% yield). Residual solvents in spectra are not peak picked. Peaks observed at 2.29, 6.78 and 6.95 ppm are the decomposition product of **2**,  $\text{Cu}_2[(2,4,6\text{-Me}_3\text{C}_6\text{H}_2\text{N})_2\text{C}(\text{H})]_2^4$ .

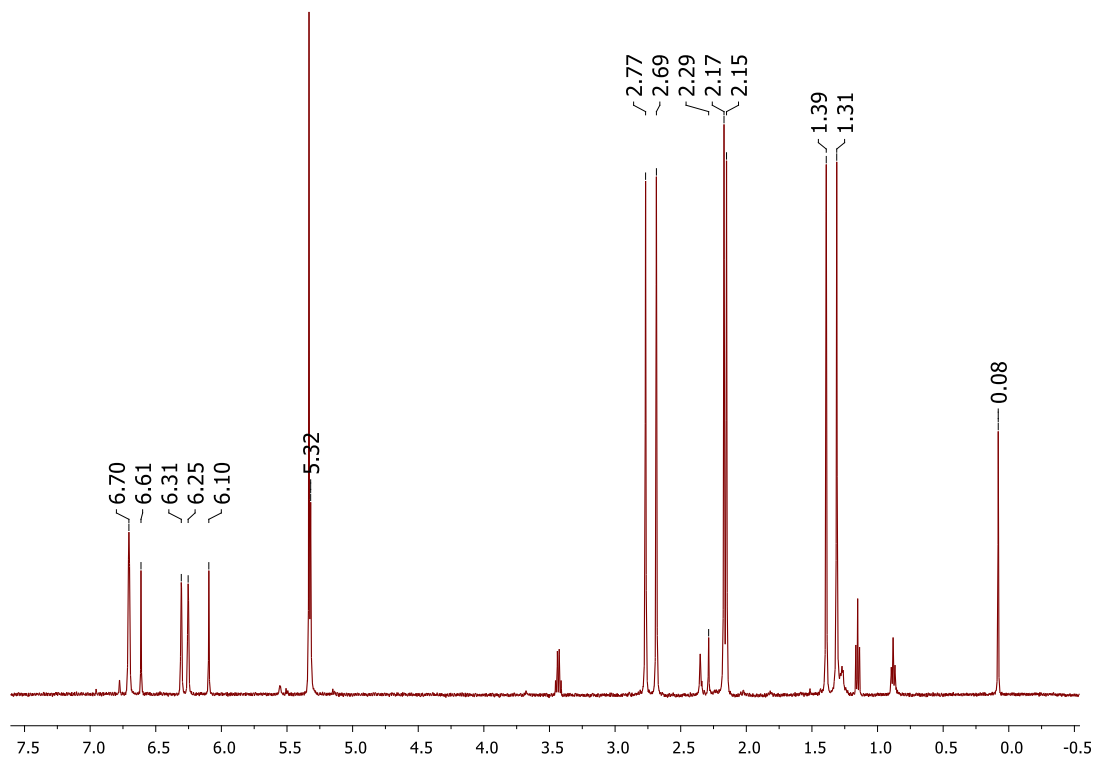


**Figure S12.**  $^1\text{H}$  NMR (500 MHz,  $\text{CD}_2\text{Cl}_2$ ) of **1** recovered after control experiment between **2** and  $\text{N}_2$  (30% decomposition). Residual solvents in spectra are not peak picked. Peak observed at 2.29 ppm is the decomposition product of **2**,  $\text{Cu}_2[(2,4,6\text{-Me}_3\text{C}_6\text{H}_2\text{N})_2\text{C}(\text{H})_2]^4$ .

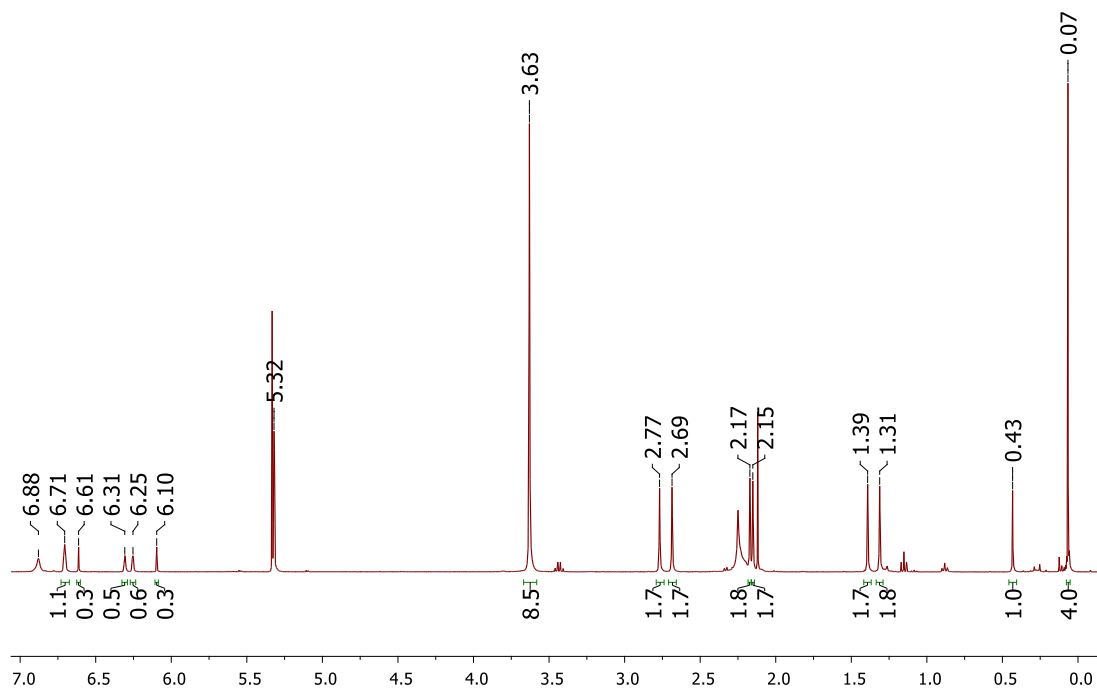


**Figure S13.** <sup>1</sup>H NMR (400 MHz, CD<sub>2</sub>Cl<sub>2</sub>) of reaction products from **2** + N<sub>2</sub>O, using 5 equivalents of TMS-Cl as an oxygen trap. Hexamethyldisiloxane appearing at 0.07 ppm is the major product and some unreacted TMS-Cl appears at 0.43 ppm. Residual solvents in spectra are not peak picked.

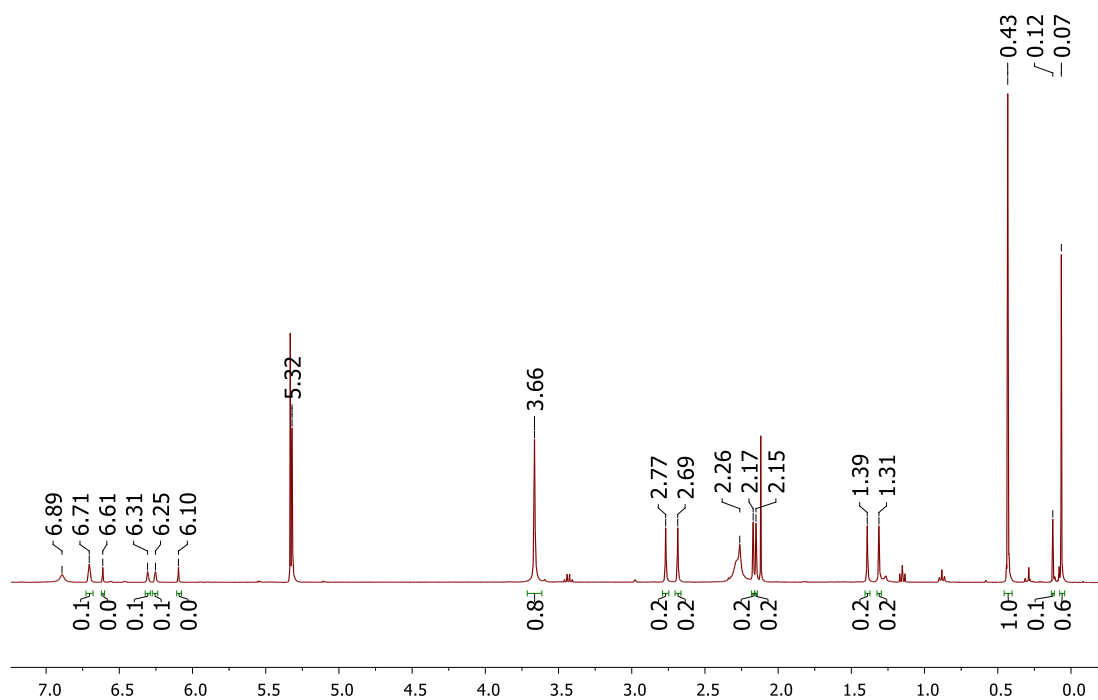


**Figure S14.** <sup>1</sup>H NMR (400 MHz, CD<sub>2</sub>Cl<sub>2</sub>) of resulting control experiment between **2** and N<sub>2</sub> and 5 equivalents of TMS-Cl. Residual solvents in spectra are not peak picked.

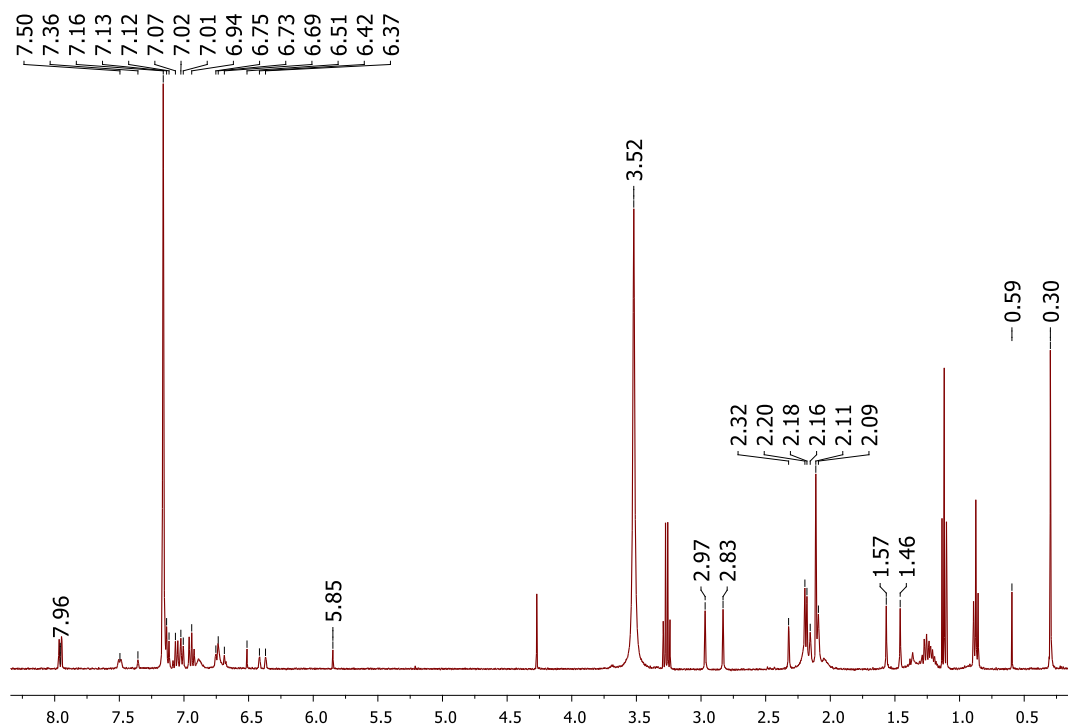


**Figure S15.**  $^1\text{H}$  NMR (400 MHz,  $\text{C}_6\text{D}_6$ ) of reaction products from **2** +  $\text{N}_2\text{O}$  using benzoyl chloride as an oxygen trap to form benzoic anhydride. Residual solvents in spectra are not peak picked.

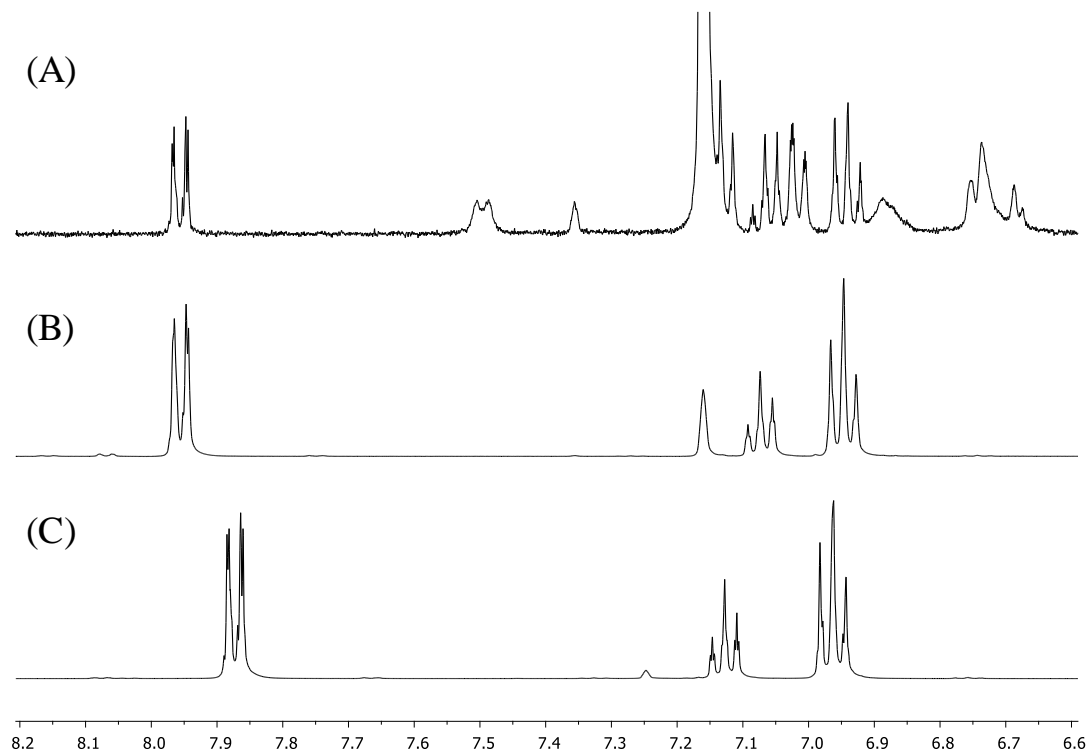


**Figure S16.** Comparison of <sup>1</sup>H NMR (400 MHz, C<sub>6</sub>D<sub>6</sub>) of reaction products from **2** + N<sub>2</sub>O using benzoyl chloride as an oxygen trap to form benzoic anhydride (A); authentic sample of benzoic anhydride (B); authentic sample of benzoyl chloride (C).

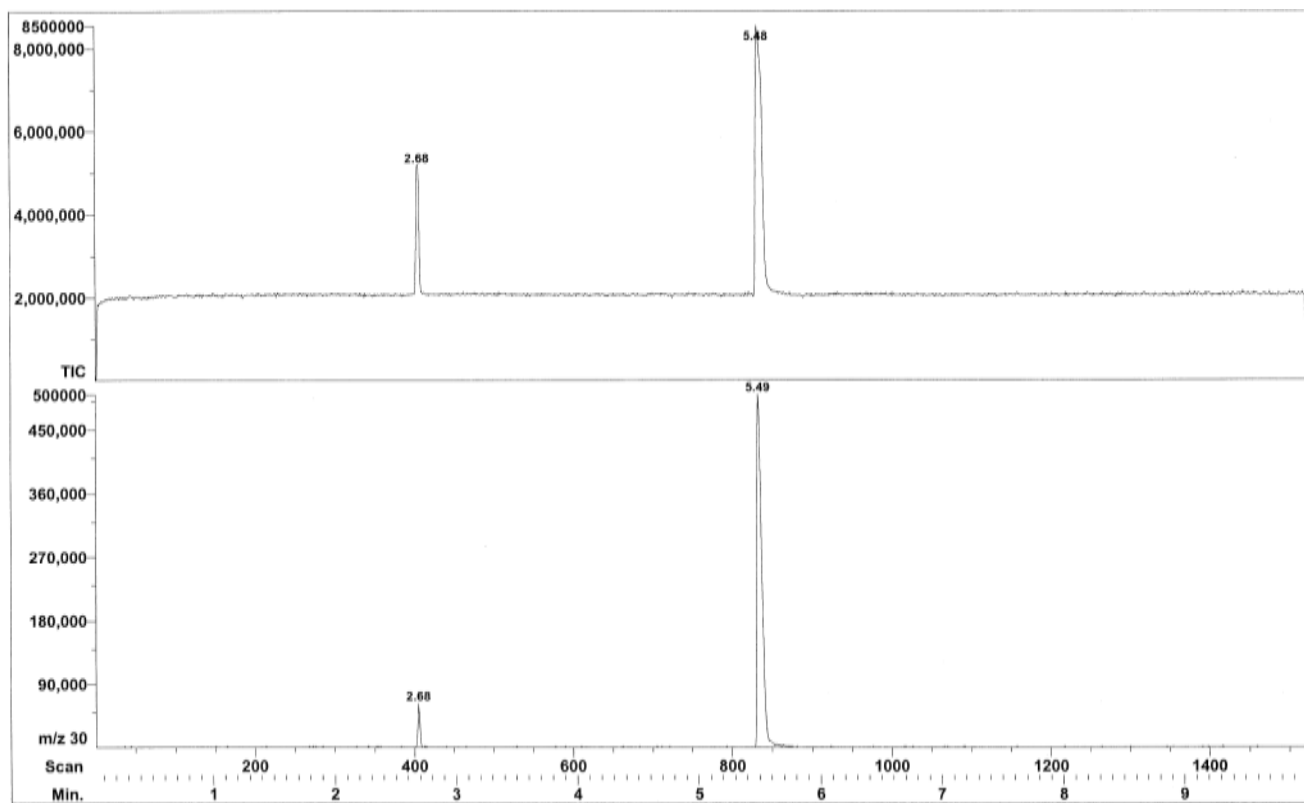


**Figure S17.** Total chromatogram (top) and extracted ion chromatogram for m/z 30 (bottom) from the reaction headspace after 48 hours of  $^{15}\text{N}_2\text{O}$  and **2**.

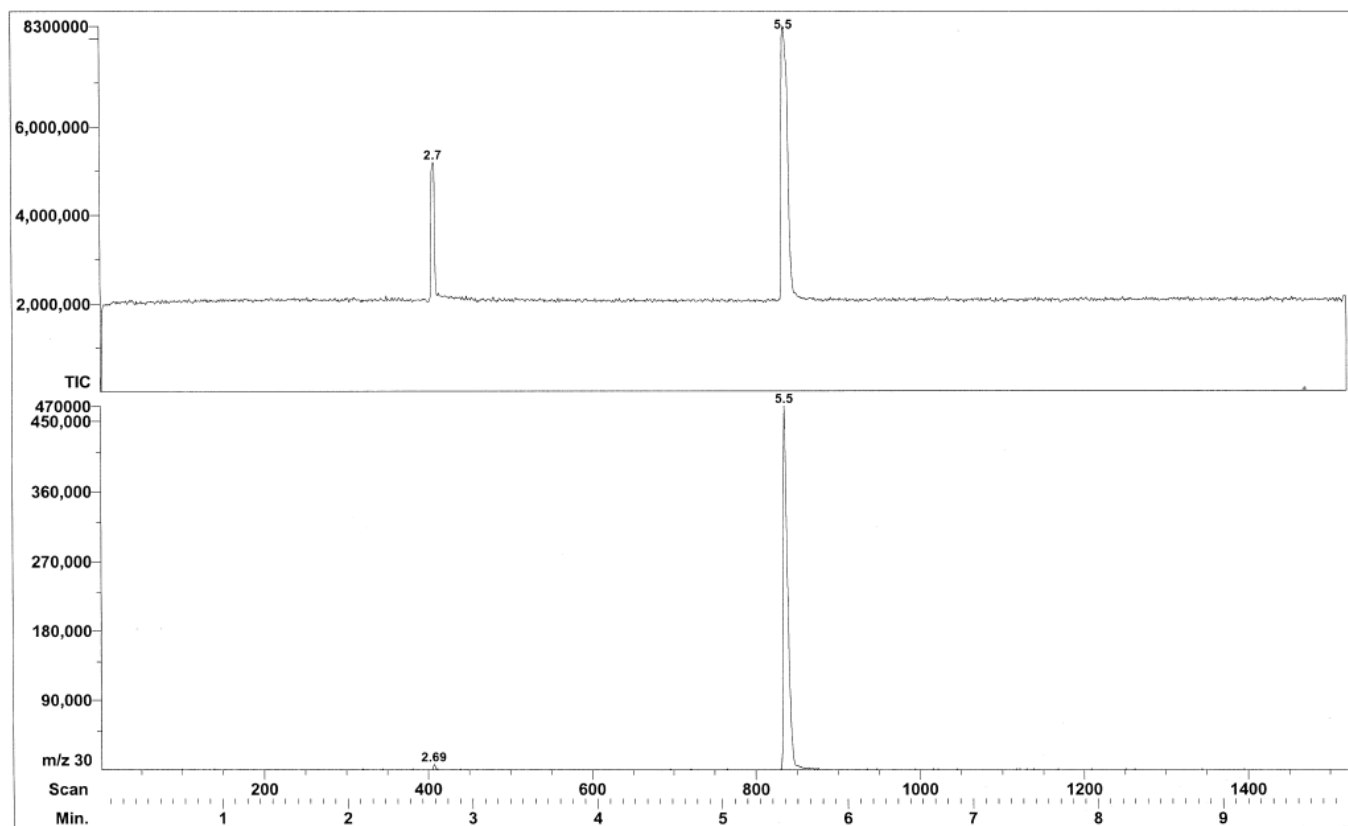


**Figure S18.** Total chromatogram (top) and extracted ion chromatogram for m/z 30 (bottom) from flask containing  $^{15}\text{N}_2\text{O}$  for 48 hours.

Scan: 405 R.T.: 2.68  
 Base: m/z 28; 100%FS #Ions: 28 TIC: 5173296 (Max Inten : 4193876)

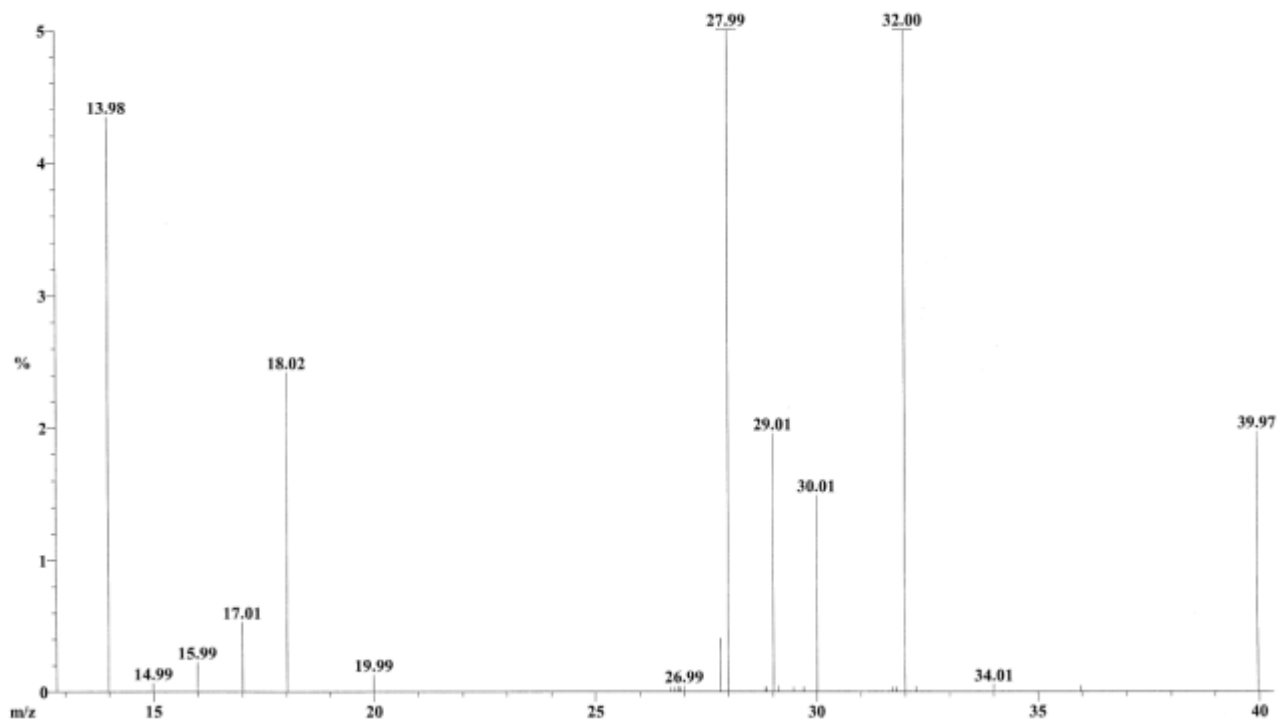


**Figure S19.** Mass spectrum of species at 2.68 minutes from the reaction headspace of  $^{15}\text{N}_2\text{O}$  and **2** after 48 hours.

**Table S1.** Percent composition of species in Figure S19.

Scan: 405 R.T.: 2.68  
 Base: m/z 28; 100%FS#Ions: 28 TIC: 5173296 (Max Inten : 4193876)

Threshold: .1% of Base

Displayed TIC: 5173296

Mass	%Base	%TIC	Intensity	Mass	%Base	%TIC	Intensity	Mass	%Base	%TIC	Intensity
13.9815	4.3	3.519	182,036	19.9908	.1	0.106	5,460	30.0124	1.5	1.209	62,548
15.9851	.2	0.182	9,428	27.8101	.4	0.328	16,980	31.9988	9.1	7.405	383,060
17.0069	.5	0.428	22,164	27.9929	100.0	81.068	4,193,876	39.9675	2.0	1.596	82,580
18.0212	2.4	1.961	101,460	29.0135	2.0	1.586	82,068				

Scan: 405 R.T.: 2.68  
 Base: m/z 28; 58.7%FS #Ions: 18 TIC: 3112296 (Max Inten : 2461140)

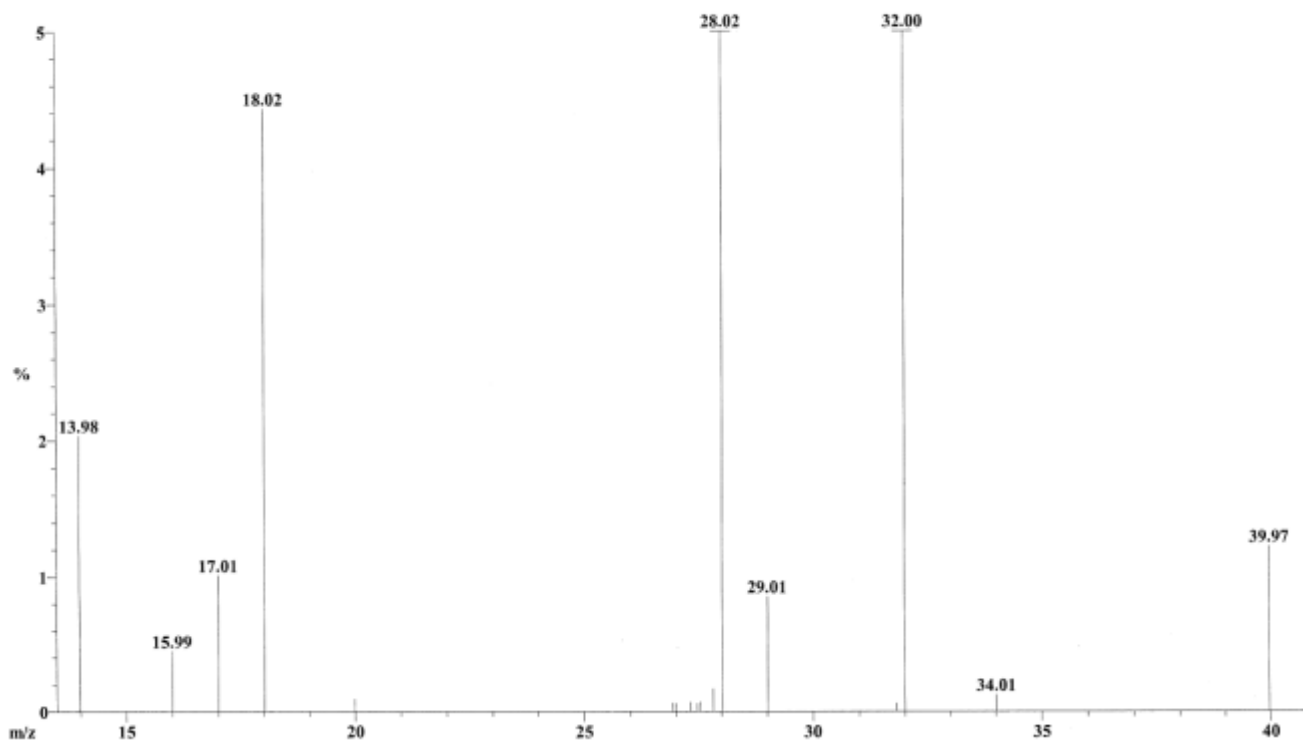


**Figure S20.** Mass spectrum of species at 2.68 minutes from a flask containing  $^{15}\text{N}_2\text{O}$  after 48 hours.

**Table S2.** Percent composition of species in Figure S20.

Scan: 406 R.T.: 2.68  
 Base: m/z 28; 100%FS#Ions: 26 TIC: 4968712 (Max Inten : 4193876)

Threshold: .1% of Base

Displayed TIC: 4968712

Mass	%Base	%TIC	Intensity	Mass	%Base	%TIC	Intensity	Mass	%Base	%TIC	Intensity
13.9815	2.9	2.468	122,644	18.0212	2.5	2.132	105,940	29.0135	1.1	0.965	47,956
15.9924	.2	0.195	9,684	27.8293	.2	0.196	9,748	31.9988	9.2	7.794	387,284
17.0069	.5	0.432	21,460	28.0121	100.0	84.406	4,193,876	39.9790	.8	0.715	35,540

Scan: 406 R.T.: 2.68  
 Base: m/z 28; 100%FS #Ions: 24 TIC: 5072672 (Max Inten : 4193876)

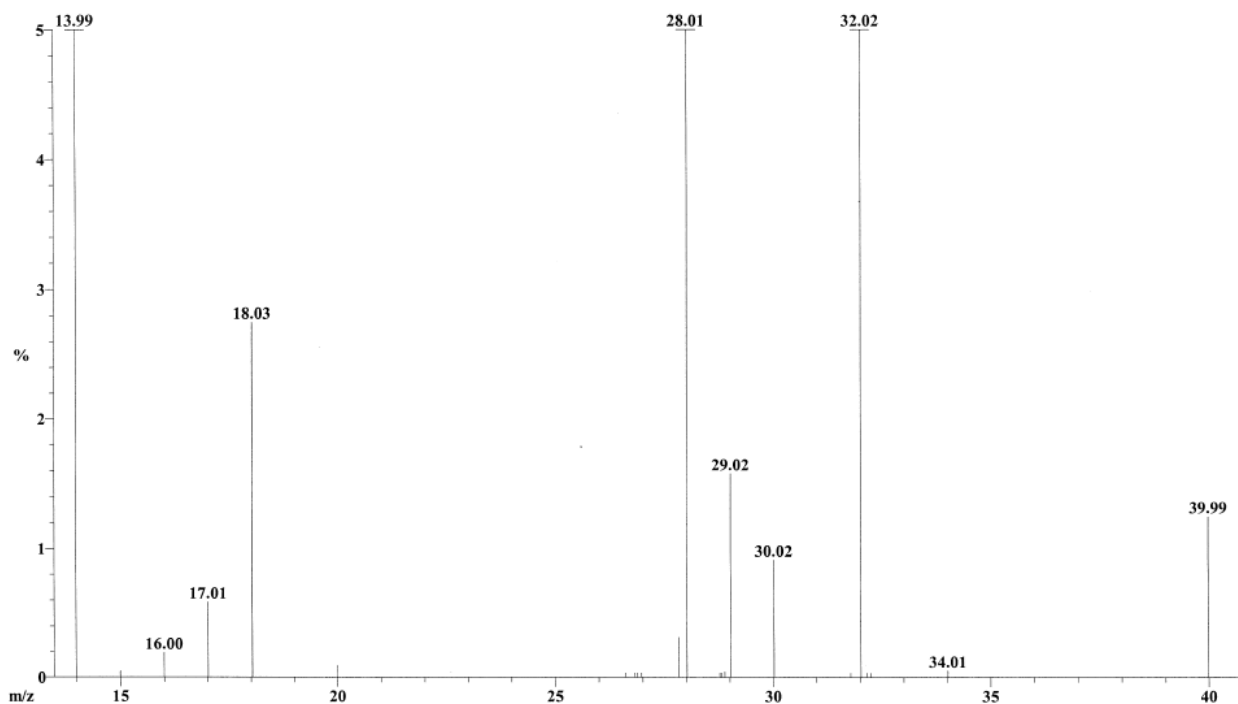


**Figure S21.** Mass spectrum of species at 2.68 minutes from the reaction headspace of  $^{15}\text{N}_2\text{O}$  and **2** after 6 hours.

**Table S3.** Percent composition of species in Figure S21.

Scan: 406 R.T.: 2.68  
 Base: m/z 28; 100%FS#Ions: 24 TIC: 5072672 (Max Inten : 4193876)

Threshold: .1% of Base

Displayed TIC: 5072672

Mass	%Base	%TIC	Intensity	Mass	%Base	%TIC	Intensity	Mass	%Base	%TIC	Intensity
13.9855	5.1	4.175	211,796	27.8257	.3	0.259	13,140	32.0156	7.7	6.338	321,492
15.9969	.2	0.158	8,020	28.0085	100.0	82.676	4,193,876	39.9904	1.3	1.034	52,436
17.0115	.6	0.484	24,532	29.0195	1.6	1.304	66,132				
18.0261	2.7	2.273	115,284	30.0185	.9	0.756	38,356				

Scan: 408 R.T.: 2.69  
 Base: m/z 28; 93.2%FS #Ions: 21 TIC: 4576356 (Max Inten : 3907156)

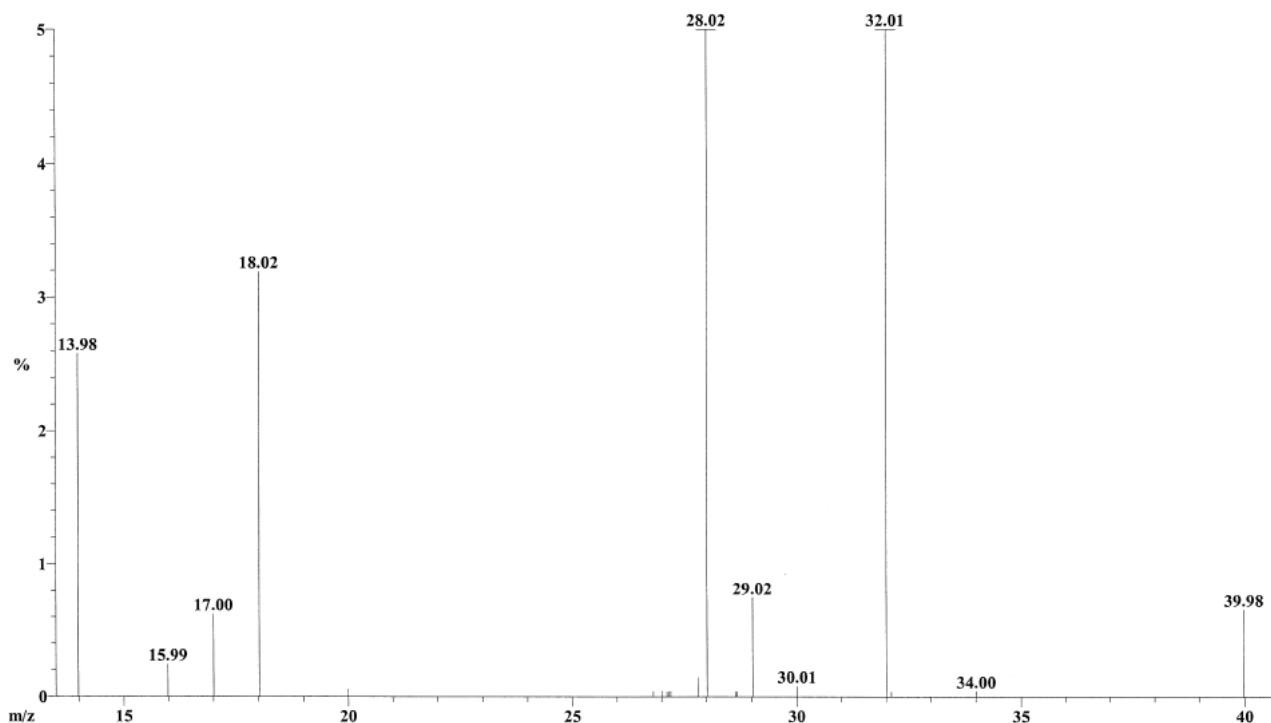


**Figure S22.** Mass spectrum of species at 2.69 minutes from flask containing  $^{15}\text{N}_2\text{O}$ .

**Table S4.** Percent composition of species in Figure S22.

Scan: 408 R.T.: 2.69  
 Base: m/z 28; 93.2%FS#Ions: 21 TIC: 4576356 (Max Inten : 3907156)

Threshold: .1% of Base

Displayed TIC: 4576356

Mass	%Base	%TIC	Intensity	Mass	%Base	%TIC	Intensity	Mass	%Base	%TIC	Intensity
13.9786	2.6	2.200	100,692	18.0183	3.2	2.722	124,564	29.0195	.7	0.638	29,204
15.9895	.2	0.206	9,428	27.8257	.1	0.125	5,716	32.0052	8.4	7.137	326,612
17.0040	.6	0.530	24,276	28.0181	100.0	85.377	3,907,156	39.9789	.7	0.561	25,684

Scan: 832 R.T.: 5.48  
 Base: m/z 46; 100%FS #Ions: 40 TIC: 8115232 (Max Inten : 4193876)

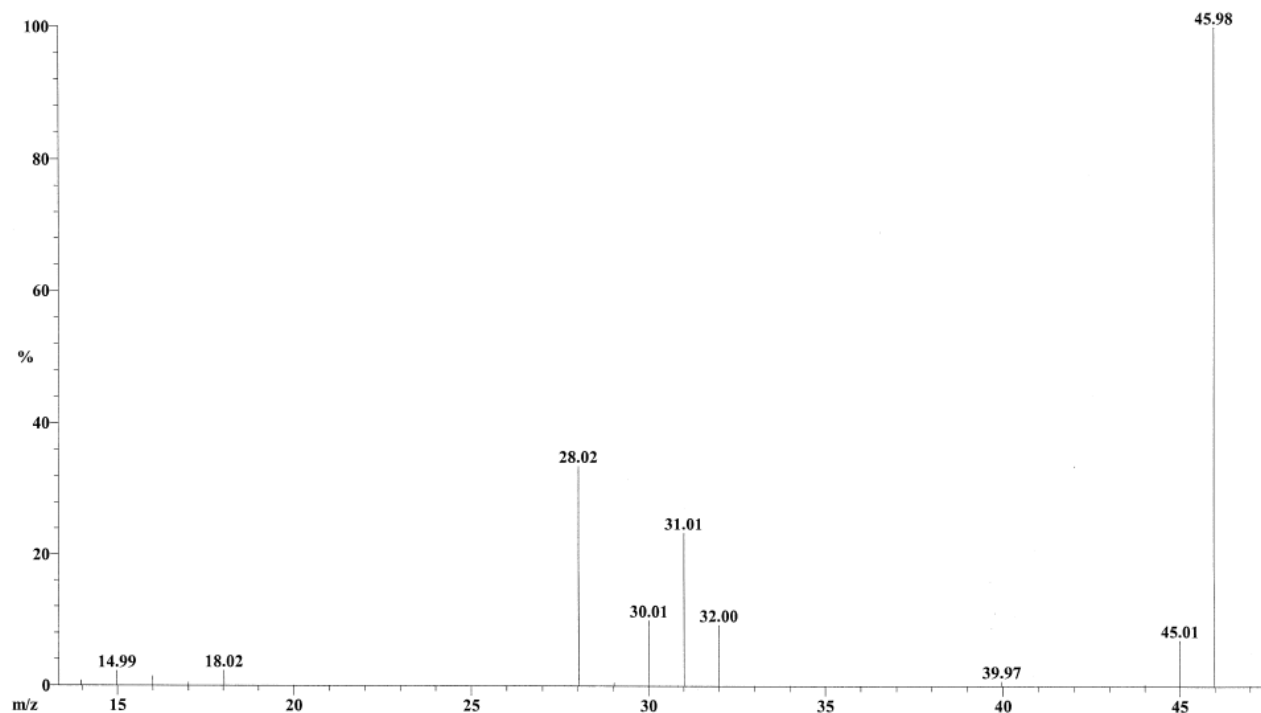


**Figure S23.** Mass spectrum of species at 5.48 minutes from the chromatogram of the reaction headspace of  $^{15}\text{N}_2\text{O}$  and **2** in Figure S17.

**Table S5.** Summary integration values of  $^{15}\text{N}_2$  from reaction headspace experiments with  $^{15}\text{N}_2\text{O}$  and **2**, after 6 and 48 hours compared to the  $^{15}\text{N}_2\text{O}$  blank. Integration values were obtained from the extracted ion chromatogram for m/z 30 for the peak with the retention time of 2.68 minutes (bottom of Figure S17 and Figure S18).

	Reaction $^{15}\text{N}_2$ Peak Integration	Blank $^{15}\text{N}_2$ Peak Integration
48 Hours	181,583	21,394
6 Hours	109,835	22,868

**Table S6.** Comparison of calculated and experimental bond distances (Å).

	<b>1'</b> (calculated)	<b>1</b> (experimental)	<b>2'</b> (calculated)	<b>2</b> (experimental)
Cu1-Cu2	2.469	2.4226(6)	2.584	2.502(1), 2.486(1)
Cu2-Cu3	2.928	3.0353(6)	2.827	2.809(1), 2.854(1)
Cu3-Cu4	2.469	2.4226(6)	2.584	2.532(1), 2.500(1)
Cu1-Cu4	2.928	3.0353(6)	2.827	2.831(1), 2.844(1)
Average Cu-S	2.261	2.180	2.302	2.217

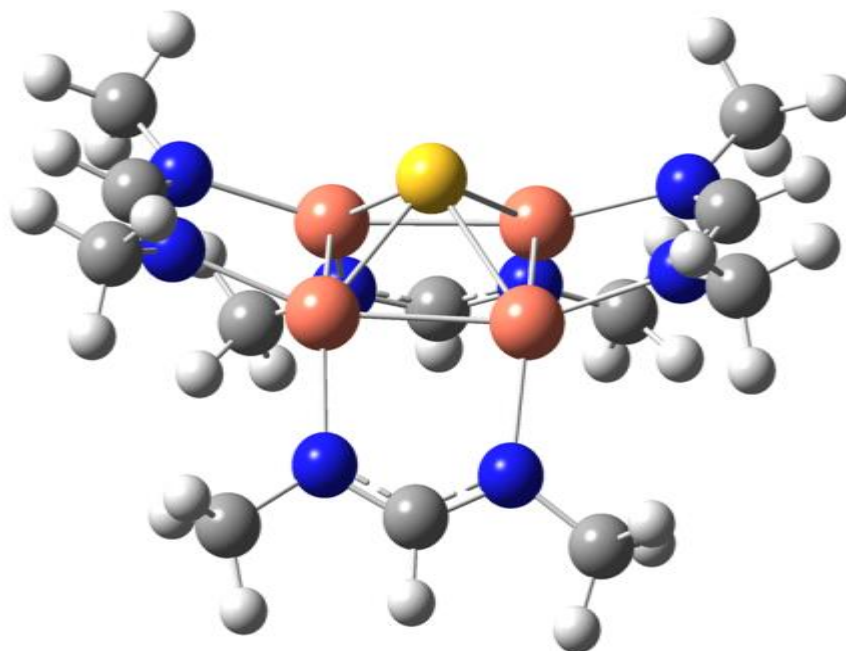


**Figure S24.** Optimized structure of 2'.

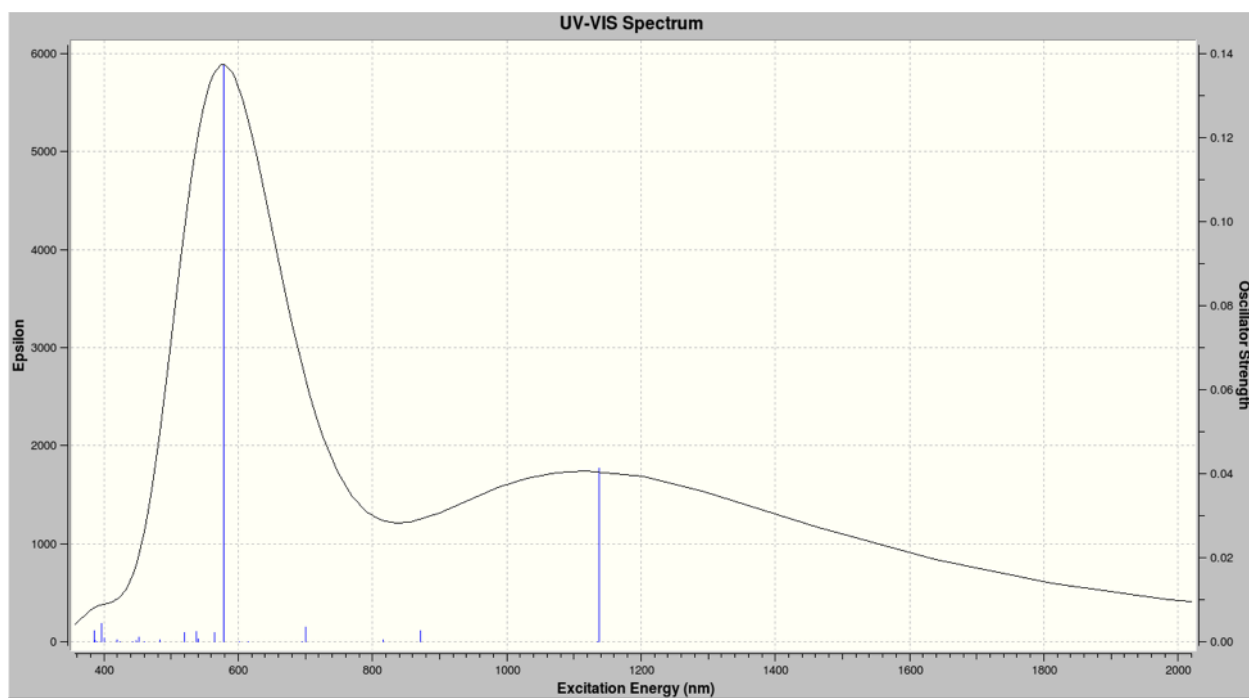


**Figure S25.** Calculated UV-Vis spectrum of 2'.

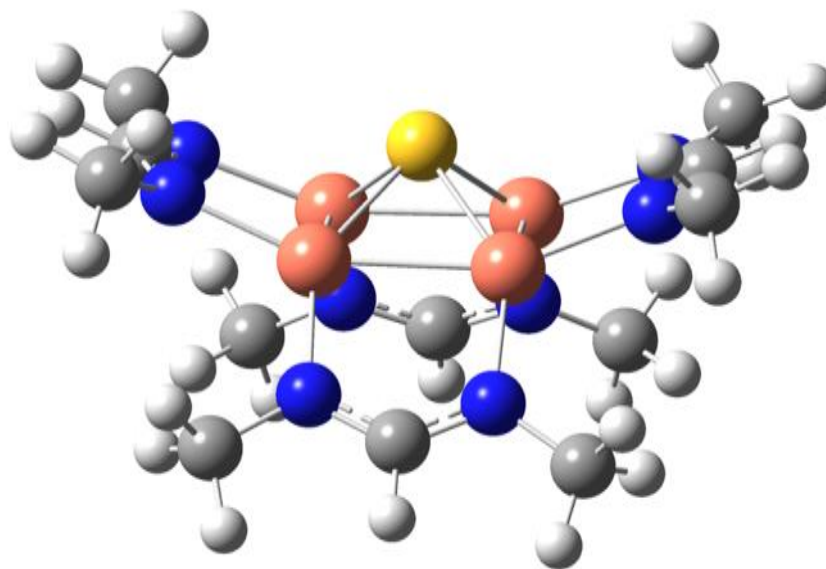


**Figure S26.** Optimized structure of 1'.

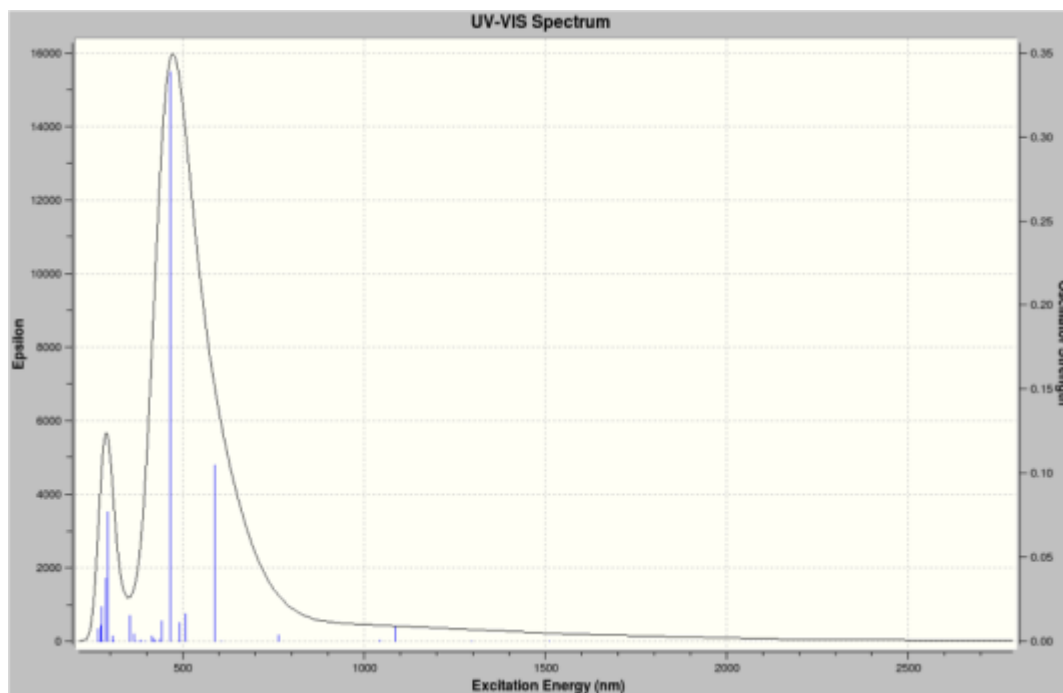


**Figure S27.** Calculated UV-Vis spectrum of 1'.

**Table S7.** Optimized coordinates of **2'**.

-----						
Center	Atomic	Atomic	Coordinates (Angstroms)			
Number	Number	Type	X	Y	Z	
-----						
1	29	0	1.386449	-1.349982	-0.224024	
2	16	0	0.000002	-0.000076	-1.474806	
3	7	0	3.281351	-0.976101	-0.923119	
4	7	0	3.126323	1.380414	-0.861635	
5	6	0	3.733485	0.243940	-1.159060	
6	1	0	4.723098	0.321561	-1.645214	
7	29	0	-1.386447	1.349952	-0.224154	
8	7	0	-3.281346	0.976012	-0.923222	
9	7	0	-3.126316	-1.380499	-0.861544	
10	6	0	-3.733473	-0.244049	-1.159074	
11	1	0	-4.723075	-0.321712	-1.645242	
12	29	0	-1.194111	-1.470350	-0.169276	
13	7	0	-0.983854	-2.734209	1.363758	
14	7	0	1.364907	-2.687537	1.258960	
15	6	0	0.218929	-3.082077	1.789964	
16	1	0	0.271111	-3.754926	2.662529	
17	29	0	1.194104	1.470329	-0.169420	
18	7	0	0.983846	2.734363	1.363467	
19	7	0	-1.364915	2.687653	1.258698	
20	6	0	-0.218937	3.082258	1.789654	
21	1	0	-0.271117	3.755185	2.662158	
22	6	0	-4.104976	2.086128	-1.378376	
23	1	0	-4.335943	2.772439	-0.551923	

24	1	0	-3.588327	2.676106	-2.150727
25	1	0	-5.062706	1.748165	-1.807901
26	6	0	-3.808144	-2.611006	-1.234625
27	1	0	-4.788424	-2.420762	-1.702280
28	1	0	-3.210188	-3.195840	-1.949527
29	1	0	-3.978270	-3.252732	-0.358617
30	6	0	-2.127197	-3.266063	2.093188
31	1	0	-2.789334	-2.456198	2.427473
32	1	0	-2.728135	-3.934564	1.460693
33	1	0	-1.820489	-3.837150	2.983909
34	6	0	2.587763	-3.192080	1.869003
35	1	0	3.264894	-2.367038	2.125869
36	1	0	2.386510	-3.760642	2.791011
37	1	0	3.133163	-3.856012	1.182523
38	6	0	4.104985	-2.086257	-1.378171
39	1	0	5.062724	-1.748332	-1.807706
40	1	0	4.335933	-2.772504	-0.551660
41	1	0	3.588346	-2.676293	-2.150485
42	6	0	3.808163	2.610891	-1.234795
43	1	0	3.978266	3.252684	-0.358834
44	1	0	4.788454	2.420608	-1.702409
45	1	0	3.210227	3.195670	-1.949759
46	6	0	2.127192	3.266324	2.092813
47	1	0	2.789424	2.456516	2.427042
48	1	0	2.728025	3.934883	1.460277
49	1	0	1.820497	3.837380	2.983559
50	6	0	-2.587772	3.192221	1.868715
51	1	0	-2.386519	3.760866	2.790672
52	1	0	-3.133196	3.856082	1.182186

53    1    0    -3.264882    2.367186    2.125659

---

**Table S8.** Optimized coordinates of **1'**.

---

Center Number	Atomic Number	Atomic Type	Coordinates (Angstroms)		
			X	Y	Z
1	29	0	1.309161	-1.408896	-0.176093
2	16	0	0.000030	-0.000018	-1.366232
3	7	0	3.123631	-1.031322	-0.923548
4	7	0	3.004493	1.333672	-0.894061
5	6	0	3.590064	0.180910	-1.162130
6	1	0	4.583731	0.236714	-1.629581
7	29	0	-1.309162	1.408912	-0.176201
8	7	0	-3.123593	1.031285	-0.923732
9	7	0	-3.004442	-1.333708	-0.894173
10	6	0	-3.590005	-0.180955	-1.162305
11	1	0	-4.583648	-0.236781	-1.629805
12	29	0	-1.157468	-1.514723	-0.152193
13	7	0	-1.027289	-2.830246	1.301666
14	7	0	1.317693	-2.747879	1.262167
15	6	0	0.167111	-3.191147	1.742215
16	1	0	0.206278	-3.905971	2.577536
17	29	0	1.157482	1.514715	-0.152169
18	7	0	1.027225	2.830266	1.301657
19	7	0	-1.317758	2.747935	1.262025
20	6	0	-0.167196	3.191189	1.742132

21	1	0	-0.206399	3.906025	2.577442
22	6	0	-3.927349	2.169324	-1.361351
23	1	0	-4.165283	2.829723	-0.518974
24	1	0	-3.385261	2.766474	-2.107040
25	1	0	-4.875848	1.848734	-1.815429
26	6	0	-3.693299	-2.557939	-1.292745
27	1	0	-4.671398	-2.346570	-1.747857
28	1	0	-3.098340	-3.120147	-2.025142
29	1	0	-3.859048	-3.212817	-0.429241
30	6	0	-2.193353	-3.416698	1.953617
31	1	0	-2.919871	-2.638329	2.215184
32	1	0	-2.700891	-4.136000	1.296463
33	1	0	-1.917232	-3.945138	2.877449
34	6	0	2.543713	-3.261118	1.863637
35	1	0	3.231249	-2.439063	2.094298
36	1	0	2.339983	-3.804238	2.797769
37	1	0	3.065933	-3.948915	1.184318
38	6	0	3.927278	-2.169374	-1.361332
39	1	0	4.875974	-1.848822	-1.815025
40	1	0	4.164834	-2.830094	-0.519102
41	1	0	3.385291	-2.766176	-2.107378
42	6	0	3.693513	2.557897	-1.292372
43	1	0	3.859656	3.212442	-0.428686
44	1	0	4.671436	2.346476	-1.747840
45	1	0	3.098468	3.120487	-2.024398
46	6	0	2.193256	3.416734	1.953655
47	1	0	1.917091	3.945163	2.877480
48	1	0	2.919775	2.638376	2.215245
49	1	0	2.700804	4.136048	1.296524

50	6	0	-2.543802	3.261181	1.863439
51	1	0	-2.340102	3.804360	2.797543
52	1	0	-3.066019	3.948928	1.184067
53	1	0	-3.231328	2.439128	2.094135

-----

**Table S9.** Excitation energies and oscillator strengths calculated for **2'**.

Excited State 1: 2.012-A 1.0901 eV 1137.34 nm f=0.0412 <S\*\*2>=0.762

124B ->125B 0.98494

Excited State 2: 2.014-A 1.0920 eV 1135.44 nm f=0.0000 <S\*\*2>=0.764

116B ->125B -0.27982

123B ->125B 0.95099

Excited State 3: 2.014-A 1.4216 eV 872.17 nm f=0.0026 <S\*\*2>=0.764

106B ->125B -0.17953

115B ->125B -0.14311

119B ->125B -0.14966

122B ->125B 0.95136

Excited State 4: 2.016-A 1.5197 eV 815.85 nm f=0.0004 <S\*\*2>=0.766

117B ->125B -0.28839

119B ->125B 0.93398

122B ->125B 0.14766

Excited State 5: 2.014-A 1.7681 eV 701.21 nm f=0.0035 <S\*\*2>=0.764

106B ->125B -0.12989

108B ->125B -0.21992

121B ->125B 0.95954

Excited State 6: 2.014-A 1.7853 eV 694.48 nm f=0.0001 <S\*\*2>=0.764

103B ->125B -0.13558

110B ->125B -0.12442

120B ->125B 0.96831

Excited State 7: 2.018-A 2.0145 eV 615.45 nm f=0.0000 <S\*\*2>=0.768

107B ->125B -0.11607

116B ->125B 0.31707

118B ->125B 0.91674

Excited State 8: 2.017-A 2.0629 eV 601.01 nm f=0.0000 <S\*\*2>=0.767

107B ->125B -0.17133

114B ->125B -0.38394

116B ->125B 0.82481

118B ->125B -0.28052

123B ->125B 0.23153

Excited State 9: 2.009-A 2.1445 eV 578.16 nm f=0.1373 <S\*\*2>=0.759

117B ->125B 0.92381

119B ->125B 0.28993

Excited State 10: 2.019-A 2.1931 eV 565.35 nm f=0.0021 <S\*\*2>=0.770

106B ->125B -0.10521

115B ->125B 0.97445

122B ->125B 0.12177

Excited State 11: 2.021-A 2.2968 eV 539.81 nm f=0.0006 <S\*\*2>=0.771

113B ->125B -0.41552  
114B ->125B 0.81505  
116B ->125B 0.25767  
118B ->125B -0.18268  
123B ->125B 0.12055

Excited State 12: 2.023-A 2.3075 eV 537.30 nm f=0.0024 <S\*\*2>=0.773

101B ->125B 0.14150  
103B ->125B 0.16943  
113B ->125B 0.86179  
114B ->125B 0.39427  
116B ->125B 0.13180

Excited State 13: 2.022-A 2.3845 eV 519.95 nm f=0.0022 <S\*\*2>=0.772

108B ->125B 0.20952  
112B ->125B 0.96306

Excited State 14: 2.022-A 2.5655 eV 483.27 nm f=0.0004 <S\*\*2>=0.772

110B ->125B -0.50719  
111B ->125B 0.84862

Excited State 15: 2.021-A 2.6971 eV 459.70 nm f=0.0000 <S\*\*2>=0.771

103B ->125B -0.22846  
110B ->125B 0.81149  
111B ->125B 0.49847  
120B ->125B 0.11851

Excited State 16: 2.024-A 2.7419 eV 452.18 nm f=0.0011 <S\*\*2>=0.774

108B ->125B -0.15892

109B ->125B 0.96425

Excited State 17: 2.027-A 2.7674 eV 448.02 nm f=0.0002 <S\*\*2>=0.778

108B ->125B 0.91836

109B ->125B 0.17454

112B ->125B -0.20170

121B ->125B 0.22317

122B ->125B -0.11180

Excited State 18: 2.026-A 2.8010 eV 442.65 nm f=0.0000 <S\*\*2>=0.776

105B ->125B 0.65387

107B ->125B 0.72969

116B ->125B 0.10957

Excited State 19: 2.028-A 2.9282 eV 423.41 nm f=0.0000 <S\*\*2>=0.778

105B ->125B 0.73661

107B ->125B -0.62098

116B ->125B -0.17680

123B ->125B -0.11599

Excited State 20: 2.026-A 2.9584 eV 419.09 nm f=0.0004 <S\*\*2>=0.776

104B ->125B 0.97627

106B ->125B 0.15190

Excited State 21: 2.023-A 3.0904 eV 401.20 nm f=0.0009 <S\*\*2>=0.773

102B ->125B -0.16140

104B ->125B -0.14710

106B ->125B 0.93325

121B ->125B 0.12978

122B ->125B	0.19626
Excited State 22: 2.027-A	3.1250 eV 396.74 nm f=0.0044 <S**2>=0.777
102B ->125B	0.96600
106B ->125B	0.15586
Excited State 23: 2.865-A	3.1862 eV 389.13 nm f=0.0000 <S**2>=1.802
124B ->126B	0.96849
124B ->130B	-0.17849
Excited State 24: 2.032-A	3.2040 eV 386.96 nm f=0.0002 <S**2>=0.783
125A ->126A	0.97670
125A ->130A	0.12024
Excited State 25: 2.025-A	3.2162 eV 385.50 nm f=0.0026 <S**2>=0.775
101B ->125B	-0.16399
103B ->125B	0.92412
110B ->125B	0.19048
113B ->125B	-0.14148
120B ->125B	0.19548

**Table S10.** Excitation energies and oscillator strengths calculated for **1'**.

Excited State 1: Singlet-A	0.8195 eV 1512.85 nm f=0.0000 <S**2>=0.000
124 ->125	0.69812
Excited State 2: Singlet-A	0.9557 eV 1297.26 nm f=0.0002 <S**2>=0.000
120 ->125	-0.12684

122 ->125 0.34619

123 ->125 0.59919

Excited State 3: Singlet-A 1.1420 eV 1085.69 nm f=0.0089 <S\*\*2>=0.000

120 ->125 0.21827

122 ->125 0.59859

123 ->125 -0.30230

Excited State 4: Singlet-A 1.1876 eV 1044.00 nm f=0.0005 <S\*\*2>=0.000

121 ->125 0.70440

Excited State 5: Singlet-A 1.6223 eV 764.26 nm f=0.0038 <S\*\*2>=0.000

118 ->125 -0.32957

119 ->125 0.62069

Excited State 6: Singlet-A 2.0442 eV 606.51 nm f=0.0000 <S\*\*2>=0.000

113 ->125 0.10210

116 ->125 -0.48352

117 ->125 0.48766

124 ->125 0.10386

Excited State 7: Singlet-A 2.1103 eV 587.53 nm f=0.1047 <S\*\*2>=0.000

115 ->125 -0.14336

120 ->125 0.64006

122 ->125 -0.12524

123 ->125 0.21890

120 <-125 -0.11134

Excited State 8: Singlet-A 2.4436 eV 507.39 nm f=0.0163 <S\*\*2>=0.000

115 ->125 0.68200

120 ->125 0.12697

Excited State 9: Singlet-A 2.5187 eV 492.26 nm f=0.0000 <S\*\*2>=0.000

113 ->125 0.66734

116 ->125 0.19973

Excited State 10: Singlet-A 2.5267 eV 490.71 nm f=0.0111 <S\*\*2>=0.000

100 ->125 -0.13704

104 ->125 -0.12763

114 ->125 0.66842

Excited State 11: Singlet-A 2.6557 eV 466.86 nm f=0.3389 <S\*\*2>=0.000

112 ->125 -0.10268

118 ->125 0.60542

119 ->125 0.31790

Excited State 12: Singlet-A 2.6650 eV 465.23 nm f=0.0000 <S\*\*2>=0.000

108 ->125 -0.14988

113 ->125 -0.18960

116 ->125 0.43924

117 ->125 0.47689

Excited State 13: Singlet-A 2.8013 eV 442.60 nm f=0.0123 <S\*\*2>=0.000

107 ->125 0.18044

110 ->125 0.66256

120 ->125 0.10742

Excited State 14: Singlet-A 2.8478 eV 435.36 nm f=0.0010 <S\*\*2>=0.000

109 ->125 0.43980

111 ->125 0.54322

Excited State 15: Singlet-A 2.9437 eV 421.19 nm f=0.0006 <S\*\*2>=0.000

101 ->125 -0.12153

104 ->125 -0.20509

109 ->125 0.50894

111 ->125 -0.42265

Excited State 16: Singlet-A 2.9488 eV 420.45 nm f=0.0018 <S\*\*2>=0.000

112 ->125 0.68901

Excited State 17: Singlet-A 2.9848 eV 415.39 nm f=0.0034 <S\*\*2>=0.000

107 ->125 0.66881

110 ->125 -0.19805

Excited State 18: Singlet-A 3.1279 eV 396.38 nm f=0.0000 <S\*\*2>=0.000

103 ->125 0.14705

108 ->125 0.66723

116 ->125 0.11342

Excited State 19: Singlet-A 3.2227 eV 384.72 nm f=0.0006 <S\*\*2>=0.000

105 ->125 0.56403

106 ->125 -0.41055

Excited State 20: Singlet-A 3.2489 eV 381.62 nm f=0.0001 <S\*\*2>=0.000

105 ->125 0.40875

106 ->125 0.56155

Excited State 21: Singlet-A 3.3478 eV 370.35 nm f=0.0000 <S\*\*2>=0.000

103 ->125 0.68142

108 ->125 -0.12975

Excited State 22: Singlet-A 3.3857 eV 366.19 nm f=0.0043 <S\*\*2>=0.000

101 ->125 -0.20671

104 ->125 0.64012

109 ->125 0.13061

Excited State 23: Singlet-A 3.5036 eV 353.88 nm f=0.0152 <S\*\*2>=0.000

102 ->125 0.68398

Excited State 24: Singlet-A 4.0030 eV 309.73 nm f=0.0000 <S\*\*2>=0.000

120 ->126 0.12598

122 ->126 -0.18612

123 ->126 0.66239

Excited State 25: Singlet-A 4.0195 eV 308.46 nm f=0.0032 <S\*\*2>=0.000

124 ->126 0.69794

Excited State 26: Singlet-A 4.0779 eV 304.04 nm f=0.0000 <S\*\*2>=0.000

122 ->126 0.66474

123 ->126 0.18888

Excited State 27: Singlet-A 4.2220 eV 293.66 nm f=0.0769 <S\*\*2>=0.000

121 ->126 0.69025

Excited State 28: Singlet-A 4.2988 eV 288.42 nm f=0.0372 <S\*\*2>=0.000

98 ->125 0.10538

100 ->125 0.26640  
101 ->125 0.56354  
104 ->125 0.12178  
109 ->125 0.14037  
114 ->125 0.16931

Excited State 29: Singlet-A 4.4764 eV 276.97 nm f=0.0000 <S\*\*2>=0.000

120 ->126 -0.29542  
123 ->127 0.60347

Excited State 30: Singlet-A 4.4959 eV 275.77 nm f=0.0206 <S\*\*2>=0.000

123 ->129 0.10267  
124 ->127 0.68345

Excited State 31: Singlet-A 4.5198 eV 274.31 nm f=0.0094 <S\*\*2>=0.000

89 ->125 0.25955  
92 ->125 0.15191  
94 ->125 0.11845  
95 ->125 0.39205  
99 ->125 0.46736

Excited State 32: Singlet-A 4.5363 eV 273.32 nm f=0.0000 <S\*\*2>=0.000

96 ->125 -0.15886  
97 ->125 0.25528  
120 ->126 0.53293  
122 ->127 -0.10522  
123 ->127 0.25643

Excited State 33: Singlet-A 4.5538 eV 272.26 nm f=0.0000 <S\*\*2>=0.000

120 ->126 0.10775  
121 ->128 0.10769  
122 ->127 0.66340  
122 ->133 0.11466

Excited State 34: Singlet-A 4.6004 eV 269.51 nm f=0.0000 <S\*\*2>=0.000

87 ->125 0.12315  
90 ->125 0.26954  
96 ->125 -0.27646  
97 ->125 0.43600  
120 ->126 -0.28827  
123 ->127 -0.13393

Excited State 35: Singlet-A 4.6488 eV 266.70 nm f=0.0072 <S\*\*2>=0.000

99 ->125 -0.11687  
121 ->127 0.64920  
121 ->133 0.10600  
122 ->128 0.17017

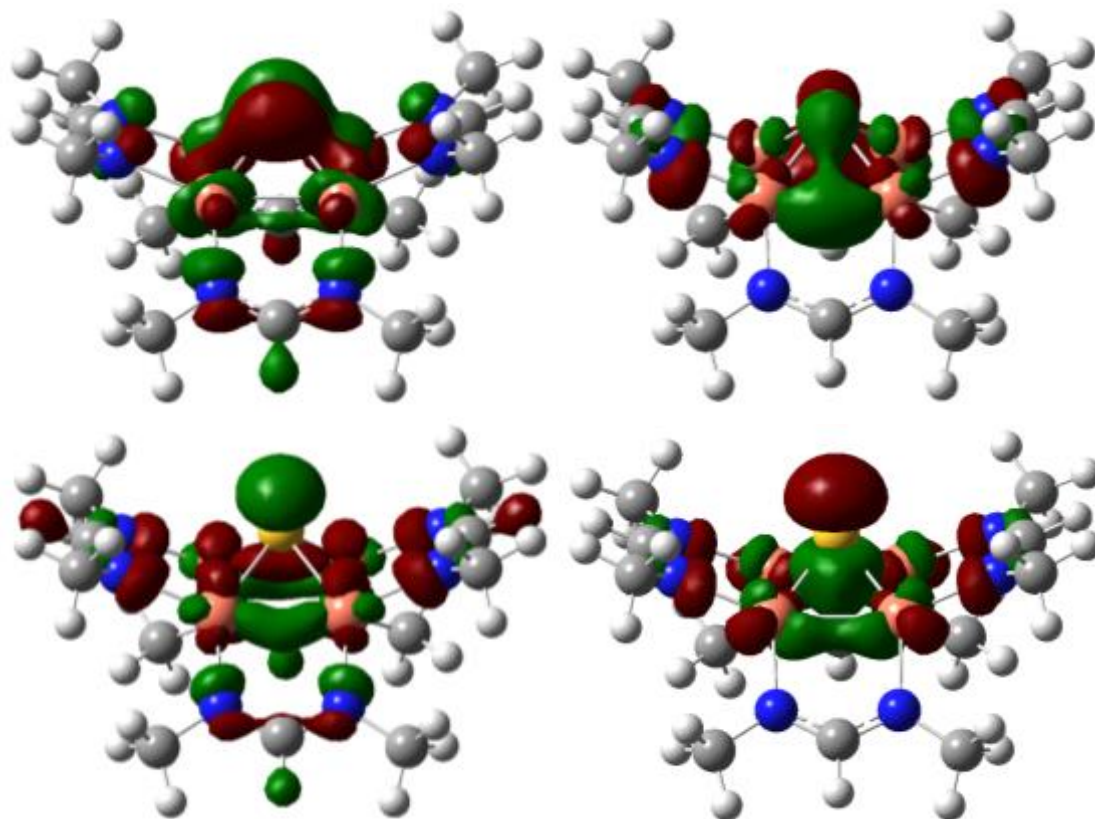


**Figure S28.** Frontier S(p) donor MOs for singlet 1': MOs 116-119 (i.e. HOMO-6 through HOMO-9; isovalue = 0.04).

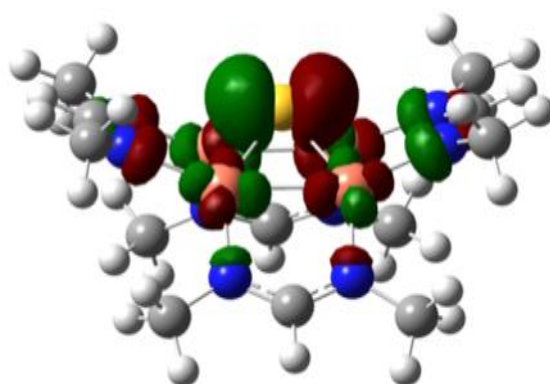


**Figure S29.** LUMO for singlet 1' (MO 125, isovalue = 0.04).

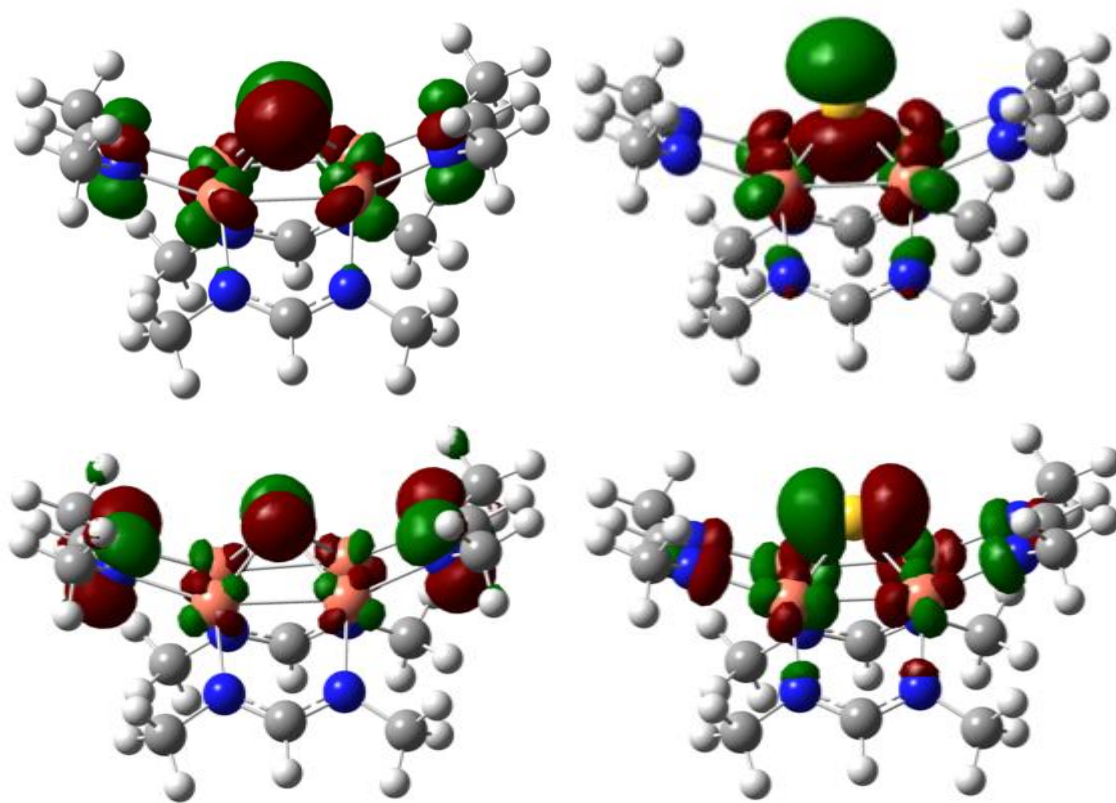


**Figure S30.** Filled S(p)  $\alpha$ -MOs for singlet  $1'$ : MOs  $118\alpha$ ,  $120\alpha$ ,  $124\alpha$ ,  $125\alpha$  (isovalue = 0.04).

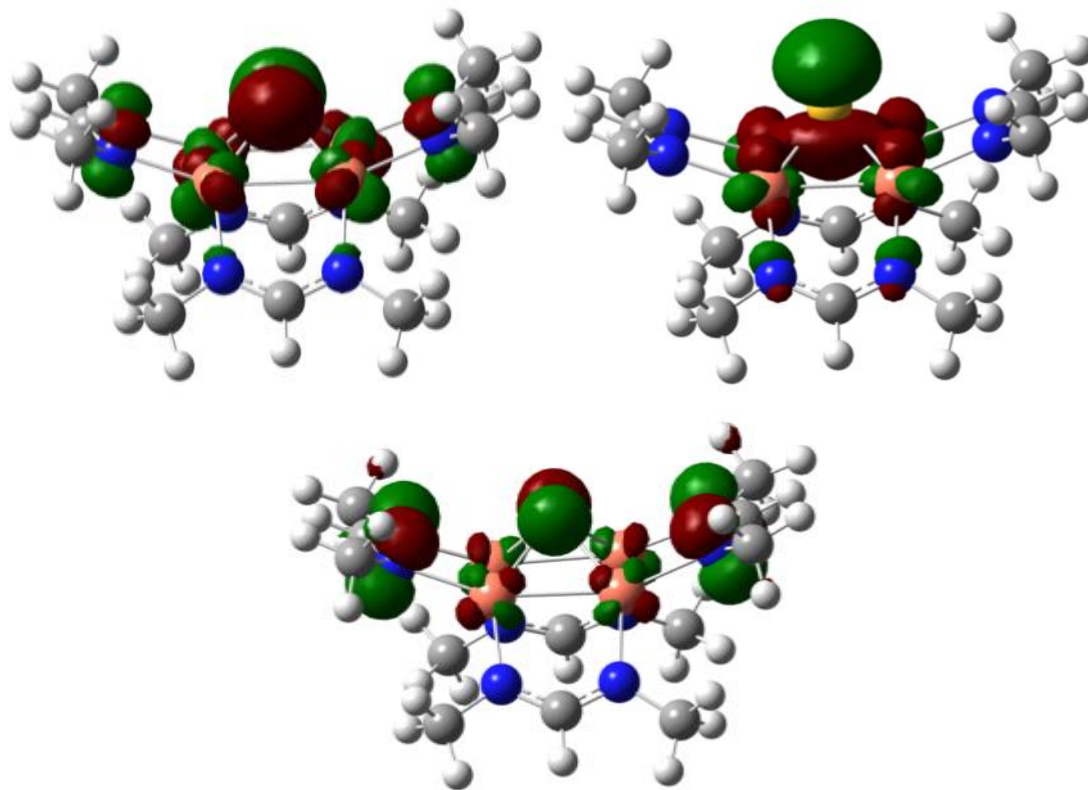


**Figure S31.** Filled S(p)  $\beta$ -MOs for singlet **1'**: MOs 116 $\beta$ , 119 $\beta$ , 123 $\beta$  (isovalue = 0.04).

### References Cited:

- <sup>1</sup> Stoll, S.; Schweiger, A. J.; *J. Magn. Reson.* **2006**, *78*, 42.
- <sup>2</sup> Sheldrick, G. M. *Acta Cryst.* **2008**, *A64*, 112–122
- <sup>3</sup> Dolomanov, O. V.; Bourhis, L. J.; Gildea, R. J.; Howard, J. A. K.; Puschmann, H. *J. Appl. Cryst.* **2009**, *42*, 339–341
- <sup>4</sup> Johnson, B. J.; Antholine, W. E.; Lindeman, S. V.; Mankad, N.P. *Chem. Commun.* **2015**, *51*, 11860.
- <sup>5</sup> Karunananda, M. K.; Vazquez, F. X.; Alp, E. E.; Bi, W.; Chattopadhyay, S.; Shibata, T.; Mankad, N. P. *Dalton Trans.* **2014**, *43*, 13361.
- <sup>6</sup> Frisch, M. J.; Trucks, G. W.; Schlegel, H. B.; Scuseria, G. E.; Robb, M. A.; Cheeseman, J. R.; Scalmani, G.; Barone, V.; Mennucci, B.; Petersson, G. A.; Nakatsuji, H.; Caricato, M.; Li, X.; Hratchian, H. P.; Izmaylov, A. F.; Bloino, J.; Zheng, G.; Sonnenberg, J. L.; Hada, M.; Ehara, M.; Toyota, K.; Fukuda, R.; Hasegawa, J.; Ishida, M.; Nakajima, T.; Honda, Y.; Kitao, O.; Nakai, H.; Vreven, T.; Montgomery, J. A., Jr.; Peralta, J. E.; Ogliaro, F.; Bearpark, M.; Heyd, J. J.; Brothers, E.; Kudin, K. N.; Staroverov, V. N.; Keith, T.; Kobayashi, R.; Normand, J.; Raghavachari, K.; Rendell, A.; Burant, J. C.; Iyengar, S. S.; Tomasi, J.; Cossi, M.; Rega, N.; Millam, J. M.; Klene, M.; Knox, J. E.; Cross, J. B.; Bakken, V.; Adamo, C.;

---

Jaramillo, J.; Gomperts, R.; Stratmann, R. E.; Yazyev, O.; Austin, A. J.; Cammi, R.; Pomelli, C.; Ochterski, J. W.; Martin, R. L.; Morokuma, K.; Zakrzewski, V. G.; Voth, G. A.; Salvador, P.; Dannenberg, J. J.; Dapprich, S.; Daniels, A. D.; Farkas, O.; Foresman, J. B.; Ortiz, J. V.; Cioslowski, J.; Fox, D. J. *Gaussian 09, Revision B.01*; Gaussian, Inc., Wallingford, CT, 2010.

- <sup>7</sup> (a) Becke, A. D. *J. Chem. Phys.* **1993**, *98*, 5648-5652. (b) Lee, C.; Yang, W.; Parr, R. G. *Phys. Rev. B* **1988**, *37*, 785-789. (c) Vosko, S. H.; Wilk, L.; Nusair, M. *Can. J. Phys.* **1980**, *58*, 1200-1211. (d) Stephens, P. J.; Devlin, F. J.; Chabalowski, C. F.; Frisch, M. J. *J. Phys. Chem.* **1994**, *98*, 11623-11627.
- <sup>8</sup> (a) Hay, P. J.; Wadt, W. R. *J. Chem. Phys.* **1985**, *82*, 299. (b) Roy, L. E.; Hay, P. J.; Martin, R. L. *J. Chem. Theory Comput.* **2008**, *4*, 1029. (c) Ehlers, A. W.; Bohme, M.; Dapprich, S.; Gobbi, A.; Hollwarth, A.; Jonas, V.; Kohler, K. F.; Stegmann, R.; Veldkamp, A.; Frenking, G. *Chem. Phys. Lett.* **1993**, *208*, 111.
- <sup>9</sup> (a) Hay, P. J.; Wadt, W. R. *J. Chem. Phys.* **1985**, *82*, 270. (b) Hay, P. J.; Wadt, W. R. *J. Chem. Phys.* **1985**, *82*, 284. (c) Hay, P. J.; Wadt, W. R. *J. Chem. Phys.* **1985**, *82*, 299.
- <sup>10</sup> Tomasi, J.; Mennucci, B.; Cammi, R. *Chem. Rev.* **2005**, *105*, 2999-3093.
- <sup>11</sup> Martin, R. L. *J. Chem. Phys.* **2003**, *118*, 4775.
- <sup>12</sup> Dennington, R.; Keith, T.; Millam, J. *GaussView, Version 4.1*; Semichem Inc., Shawnee Mission, KS, 2009.